NTNU – Trondheim
Norwegian University of
Science and Technology

Drilling in geomechanically stressed formations over and adjacent to salt domes.

Rune Vedøy

Petroleum Geoscience and Engineering
Submission date: June 2015
Supervisor: Rune Martin Holt, IPT
Co-supervisor: Olav Log, Centrica Energi
Christian Opsahl, Centrica Energi

Norwegian University of Science and Technology
Department of Petroleum Engineering and Applied Geophysics

Abstract

This thesis is in two parts:
The first part is a literature study with the intent of identifying the general behavior of stress perturbations related to some standard, often seen, salt geometries. The second part is an investigation of wellbore stability surrounding the Butch salt diapir in the South-west North Sea. From the calculations done for several different well trajectories, the effect of the salts stress perturbations gives insight into where it is best to drill, and how. These two parts where connected to give a set of guidelines for drilling close to salt diapirs such as the Butch salt diapir.

Salt structures can cause strong stress perturbations, compared to the far field, in the adjacent formations. The salts inability to sustain deviatoric stresses are the cause of these perturbations. How the stresses are distributed will be a strong factor of the geometry of the salt body. Flat allochthonous salt will have reduced minimum principal stresses above and below. Convex curves will show a decrease in minimum principal stress and therefore an increase in shear stresses, whilst concave curves will have an increased minimum principal stresses and lower shear forces due to horizontal loading from the salt. Connected salt diapirs will generally have a decrease of the minimum principal stress, hoop stress, an increase of the radial stress, maximum horizontal, whilst the vertical stress will vary depending on the density of the salt compared to the sediments surrounding it. The stress perturbations surrounding a salt body will in all likelihood lead to a re-orientation of the stress directions surrounding it. The disturbances in the stress field can extend up to 1 times the width of the salt, with the severity reducing further away from the salt. When planning to drill a well in an area with a salt body, a certain distance should be kept from the salt, especially in the upper part of a salt diapir with a high slope. If drilling is desired in the upper parts of a salt diapir, the best direction to drill would be directly towards it. The worst would be drilling parallel close to the salt. At the base of a diapir, it is expected that the stress perturbations are smaller than for the upper part, having less constrains on the well trajectory. Proper stress and material properties estimations are important close to the salt. A 3D geomechanical model is a good way of achieving relatively good stress estimations.

Abstrakt

Denne masteroppgaven er delt i to deler:
Første del er et litteraturstudie med den hensikt å identifisere den generelle oppførselen til spenningsforstyrrelser relatert til noen standard, ofte sett, salt geometrier. Andre del er en undersøkelse av brønnstabilitet rundt saltdiapiren Butch, Sør-vest i Nordsjøen. Fra utregningene gjort for flere brønnbaner, gir effekten av saltets spennings forstyrrelser innsikt i hvor det er best å bore, og hvordan. De to delene ble så brukt som bakgrunn for å gi retningslinjer til boring nære saltdiapirer, som Butch i Nordsjøen.

Salt strukturer kan forårsake store spenningsforstyrrelser, sammenlignet med normal spenningstilstand, i formasjonene ved siden av. Saltets manglende egenskap til å tåle forskjeller mellom spenningene er årsaken til disse forstyrrelsene. Hvordan spenningene er distribuert vil være sterkt avhengig av geometrien til saltkroppen. Flate alloktone saltstrukturer vil ha redusert minimum prinsipiell spenning ovenfor og nedenfor. Konvekse kurver vil ha redusert minimum prinsipiell spenning og derfor en økning i skjærspenninger, mens konkave kurver vil ha økt minimum prinsipiell spenning og lavere skjærkrefter grunnet lasting horisontalt. Saltdiapirer knyttet til kilden, vil generelt ha redusert minimum prinsipiell spenning, hoop-spenning, en økning av radiell spenning, maksimum horisontal, mens vertikalspenningen vil variere med tettheten til saltet og tettheten til formasjonene rundt. Spenningsforstyrelsene rundt en saltkropp vil med all sannsynlighet føre til en re-orientering av spenningsretningene rundt den. Forstyrrelsen i spenningsfeltet kan strekke seg så langt som 1 ganger vidden til saltet, med minkende alvorlighet lengre borte fra saltet. Under planleggingen av å bore en brønn i et området med en saltkropp, burde en viss avstand holdes fra saltet, spesielt i den øvre delen av en saltdiapir med høy helling. Om boring er ønsket i den øvre delen av en saltdiapir, er den beste retningen å bore rett mot saltet. Den verste retningen vil være å bore parallelt nær saltet. Ved basen av saltet er det forventet av spenningsforstyrrelsene er mindre enn for øvre del, og vil ha mindre restriksjoner på brønnbanen. Gode spennings og materielle egenskaper er viktige nære saltet. En 3D geomekanisk model er en god måte å få relativt gode spenningsestimater.

Preface/dedication

I would like to give my thanks to Centrica Energy for providing me with the problem for my master thesis, for all the help I have gotten during my work, and for providing me with everything I needed.
I would also like to thank my supervisor Rune Holt for guiding me through the last months, pointing me in the right direction. I appreciate your help.

Table of contents

List of figures

List of tables

Abbreviations

FADC – Fluid-assisted diffusional creep

LOT- Leak off test

SG – Specific gravity (g/cm^3)

XLOT – Extended leak off test

1. Introduction

Salt diapirs and other geometries like salt sheets, are used to describe a body of salt, which has intruded up into the overlying formations. Such an intrusion is connected to tectonic faulting or fracturing, like what is seen in extensional, contractional and strike slip regimes. The regional stress state will have a major effect on the end result of the salt shape. Shalt sheets will, for example, often be found in listric environments. With this and some sort of growth mechanism in place, for example buoyancy as a result of density differences, salt will be able to create diapirs and other salt geometries. Salt will flow as long as there is an external deviatoric stress on the salt body (Dusseault et al. 2004b). The inability to sustain deviatoric stresses, combined with the almost non-existence of permeability and porosity, causes it to be susceptible to flow at mean stresses above 5 MPa (Fredrich et al. 2003). Salt therefore wishes to reach an isotropic condition.

Some of the biggest oil fields in the world are in some way related to a salt body. The Gulf of Mexico and the North Sea are two examples of oil rich regions, with many salt structures. The salts behavior will have a major impact on the near stresses in the formations adjacent to the salt body. To exploit the rich recourses trapped up against the salt, the different geometries effect on the local stresses needs to be understood and investigated. Although each salt body will have a unique effect on the adjacent formations, it is possible to find a common trend for some idealized geometries. Many such investigations has been conducted, still the stress perturbations related to salt are not fully understood.
The introduction of 3D geomechanical models, created using programs such as Abaqus, has given a unique ability to visualize how the stresses might be affected and distributed. It is not a full proof method, but together with field data and experience it can yield a model which is close to the reality. Creating such a model will have many benefits, as it can give insight into the distribution of stresses and pore pressures, helping engineers in choosing the optimal wellbore trajectory. With the knowledge that hydrocarbons have a tendency to migrate from areas of high levels of mean or minimum principal stress, to regions with less stress (Koupriantchik et al. 2005), such a model can also be useful in choosing the areas to explore.

Drilling in or adjacent to salt has long been a challenge. The perturbed stresses can leave large regions adjacent to the salt, in which it is not possible to have a stable hole. Insight into the

stresses adjacent to the salt, the formations and the distribution of stresses is therefore important for any drilling engineer.

In this thesis the general stress perturbations and regimes associated with generalized salt geometries is examined together with the wellbore stability for different wellbore trajectories related to the Butch salt structure in the North Sea. A geomechanical study has already been conducted on Butch, making it a good example for wellbore stability calculations. With the knowledge of the more generalized stress perturbations and the wellbore stability calculations, some general guidelines are created.

2. Introduction to salt and salt domes

2.1. Stress

The ability of most materials to resist and recover from deformation produced by forces is called elasticity (Fjær et al. 2008). The theory of elasticity rests on the concepts of stress and strain. Petroleum related rock mechanics is interested in rocks with porosity and permeability, therefore the theory of poroelasticity has to be taken into account.
Stress is defined as (Fjær et al. 2008, 1):

$$\sigma = \frac{F}{A} \tag{1}$$

Where F is a force on a cross-section A.

The shear stress can be defined from the forces working on a inclined cross-section (Fjær et al. 2008):

$$\tau = \frac{F_p}{A_{inc}} \tag{2}$$

F_p is the force parallel to the inclined plane and A_{inc} is the cross-section for the inclined plane. A stressed body at rest requires that all the forces acting on it cancel out. From this we get the equations of equilibrium (Fjær et al. 2008, 6):

$$\frac{\partial \sigma_x}{\partial x} + \frac{\partial \tau_{yx}}{\partial y} + \frac{\partial \tau_{zx}}{\partial z} + \rho f_x = 0 \tag{3}$$

$$\frac{\partial y}{\partial y} + \frac{\partial \tau_{xy}}{\partial x} + \frac{\partial \tau_{zy}}{\partial z} + \rho f_y = 0 \tag{4}$$

$$\frac{\partial \sigma_z}{\partial z} + \frac{\partial \tau_{xz}}{\partial x} + \frac{\partial \tau_{yz}}{\partial z} + \rho f_z = 0 \tag{5}$$

f_x, f_y and f_z are components of gravity in the x-, y- and z-direction.

Principal stresses are normal stresses that are in the direction of which the shear stress is zero.

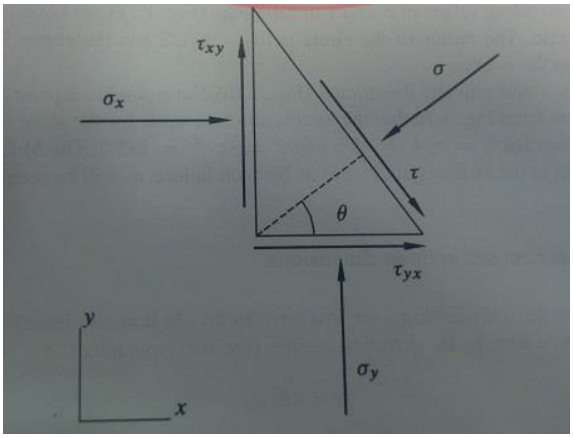

Figure 1: Force equilibrium on a triangle. The arrows show the direction of the forces (Fjær et al. 2008, 7).

For normal and shear stresses at a surface oriented normal to a general direction in the xy-plane for the triangle in figure 1 to be at rest, the cancellation of forces implies that (Fjær et al. 2008, 7):

$$\sigma = \frac{1}{2}(\sigma_x + \sigma_y) + \frac{1}{2}(\sigma_x - \sigma_y)cos2\theta + \tau_{xy}sin2\theta \tag{6}$$

$$\tau = \frac{1}{2}(\sigma_y - \sigma_x)sin2\theta + \tau_{xy}cos2\theta \tag{7}$$

$$tan2\theta = \frac{2\tau_{xy}}{\sigma_x - \sigma_y} \tag{8}$$

By solving equation 8, the directions of the principal axes of stress can be found. By inserting equation 8 into equation 6 the principal stresses in 2D, which are orthogonal, can be found (Fjær et al. 2008, 8):

$$\sigma_1 = \frac{1}{2}(\sigma_x + \sigma_y) + \sqrt{\tau_{xy}^2 + \frac{1}{4}(\sigma_x - \sigma_y)^2} \tag{9}$$

$$\sigma_2 = \frac{1}{2}(\sigma_x + \sigma_y) - \sqrt{\tau_{xy}^2 + \frac{1}{4}(\sigma_x - \sigma_y)^2} \tag{10}$$

If the principal axes are organised so that the first principal axis is parallel to the x-axis and the second principal axis is parallel to the y-axis, the stresses in a general direction θ relative to the x-axis can be given as (Fjær et al. 2008, 8):

$$\sigma = \frac{1}{2}(\sigma_1 + \sigma_2) + \frac{1}{2}(\sigma_1 - \sigma_2)cos2\theta \tag{11}$$

$$\tau = -\frac{1}{2}(\sigma_1 - \sigma_2)sin2\theta \quad (12)$$

Effective stress is defined as (Fjær et al. 2008, 33):

$$\sigma'_{ij} = \sigma_{ij} - \delta_{ij}\alpha p_f \quad (13)$$

The i and j represent the stresses in numbers, p_f is the pore pressure and δ_{ij} is the Kronecker symbol. The Kronecker symbol is zero if i is not equal to j.

2.2. Salt properties

Rock salt formations have properties which makes it a more complex task to drill in and around. Salt formations at depths have the ability to flow under deviatoric stresses, which means that as long as stress is applied the salt material will flow. The assumption that $\sigma_v = \sigma_{HMAX} = \sigma_{hmin}$ for a salt body at rest is therefore a valid assumption (Dusseault et al. 2004b). This flow, which is known as creep, causes a shrinkage over time in a wellbore, and together with plastic flow this shrinkage can cause severe problems like stuck pipe, casing collapse and loss of equipment.

Rock salt is a soluble material, and the solubility will depend on the mineralogical content of the salt and the mud or fluid used to drill the well. Salt has a high thermal conductivity coefficient, making it better at dissipating differences in temperature when compared to formations such as shale, limestone and sandstone (Dusseault et al. 2004b).

2.2.1. Composition

The composition of subsea salt formations are usually close to pure NaCl, halite. It will in most cases, to a certain degree, have impurities such as shale beds. These impurities are small and in the range of 0-15 % (Dusseault et al. 2004b). Other salts, halides, might exist as beds within the salt. Examples of relatively pure rock salt is the Tahe oilfield in the Tarim Basin in Xinjiang province in China, where the chemical content of the rock salt is estimated to be 80-90 % pure NaCl (Zhong et al. 2008). In the North Sea Zechstein salt formations, care has to be taken as thick layers of bischofite and carnallite exists (Dusseault et al. 2004b).

Other encountered salts within rock salt formations are (Håpnes 2014):

- Sulfates: Anhydrites, gypsum, langbeinite, kieserite and epsomite
- Potassium salts: Sylvite, carnallite, polyhalite and kainite
- Chlorides :Bischofite and tachyhydrite

Salt	Density (Specific gravity)	UCS (Uniaxial compressive strength)	Hardness (Mohs scale
Halite	2,17		2-2,5
Anhydrite	2,97		3,5
Gypsum	2,31-2,33		2
Carnallite	1,6		2,5
Bischofite	1,56		1,5-2
Tachyhydrite	1,66		2
Halite: www.en.wikipedia.org/wiki/Halite Anhydrite: www.en.wikipedia.org/wiki/Anhydrite#Salt_dome_cap_rocks Gypsum: www.en.wikipedia.org/wiki/Gypsum Carnallite: www.en.wikipedia.org/wiki/Carnallite Bischofite: www.en.wikipedia.org/wiki/Bischofite Tachyhydrite: www.en.wikipedia.org/wiki/Tachyhydrite			

Table 1: Characteristics of different salts

The calcium sulfate salts, anhydrite and gypsum, are some of the more common inclusions found in salt structures. Gypsum is relatively soft and easier to drill through compared to Anhydrite. Anhydrite is immobile (Costa et al. 2010). Carnallite, bischofite and tachyhydrite are also commonly found as inclusions in salt structures. These salts are very mobile compared to Halite. Figure 3 compares creep rates for halite, carnallite and tachyhydrite.

Knowing the chemical composition of the salt to be drilled is important for properties such as creep and solubility, as will be presented later in this chapter.

2.2.2. Creep

Creep is the rate of flow of visco-elastic materials as long as stress is applied on these materials for a length of time. Salt has a rather high Poisson's ratio of 0.25 - 0.5, which indicates the plastic nature of the salt. When the salt then exhibits permanent deformation for all octahedral shear stress creep develops (Omojuwa, Osisanya, and Ahmed 2011). As long as there is an external deviatoric stress on the salt body, a steady-state creep will continue as long as the crystalline fabric of the rock remains the same (Dusseault et al. 2004b). Salt is susceptible to flow at mean stresses above roughly 5 MPa (Fredrich et al. 2003). This is because salt, pure halite, starts with a specific gravity of 2.16 g/cm^3, most likely higher because of impurities, whilst the surrounding sediments will have higher densities. The exact depth when the overburden becomes denser than salt will vary with porosity and type of rock. The specific gravity will not increase for the salt as its low porosity will prevent it from becoming more dense, but it will do so for the surrounding formations (Omojuwa, Osisanya, and Ahmed 2011). Salt permeability is close to zero and the porosity can become as low as 0.3-1.5 % (Dusseault et al. 2004b). These low values for porosity and permeability are responsible for the tendency of plastic and creep behavior at low stress levels (Omojuwa, Osisanya, and Ahmed 2011).

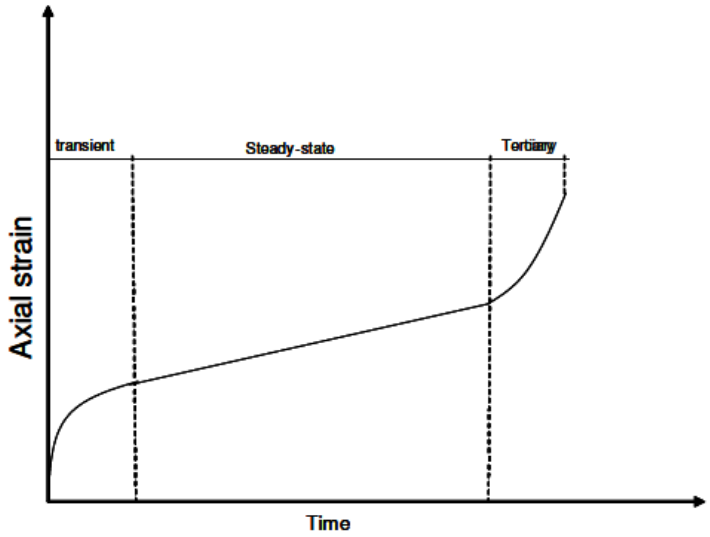

Figure 2: A typical axial creep deformation curve (Costa et al. 2010).

The typical curve for axial creep deformation curve is illustrated in Figure 2. The two first stages will always occur when drilling in salt, the third might happen depending on the temperature and the differential stress (Costa et al. 2010). For the purposes of drilling Dusseau et al. (2014) argued that the transient creep can be ignored as it is has no consequences for the borehole, this is done for practical purposes. With all this in mind the creep can be expressed as (Dusseault et al. 2004b):

$$\frac{d\varepsilon}{dt} = A\left(\frac{\sigma - p_b}{\sigma_o}\right)^n e^{\frac{-Q}{RT}} \tag{14}$$

dε/dt is the steady-state strain rate, A is a constant determined through calibration, σ-p_b is the difference between in situ stress σ borehole pressure p_b, Q is the Arrhenius thermal activation energy for creep and n is a constant determined from experimental data. σ_o is a normalizing stress value.

The Arrhenius thermal activation term it is recommended to use a value of 95 kJ/mole, σ_o is commonly taken as 10 MPa and the exponent n has by back-analyses from mines and other studies been suggested to have a value of 3. The value for n is not necessarily the only viable option, for the deep salt formation wells drilled in the Tahe oilfield in China the value used for n was 4.5 (Zhong et al. 2008).

The creep strain rate will be affected by composition, impurities, the differential stress applied to the salt, temperature and the water content (Costa et al. 2010).
The temperature will lower the plastic and elastic strain rate, and also the plastic mean stress. This means the salt body will creep at lower differential stresses (Omojuwa, Osisanya, and Ahmed 2011). The water content can create an effect known as FADC, fluid-assisted diffusional creep. It appears to be a critical component of the mechanisms that control creep (Dusseault et al. 2004b).

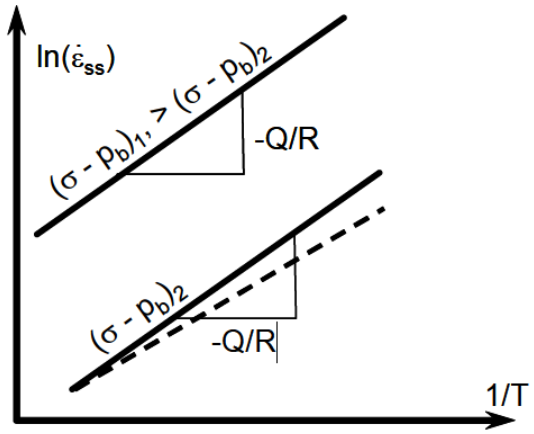

Figure 3: Temperature effect on creep (Dusseault et al. 2004b).

In figure 3 the typical creep behavior for halite, carnallite and tachyhydrite are shown at a temperature of 86ºC and σ_o = 10 MPa. The axial strains shown were accumulated over a 160 hour long testing time. Here tachyhydrite is shown to creep 107 times faster than halite, and 2,7 times faster than carnallite (Costa et al. 2010).

These results show the importance of being aware of the mineralogical composition of the salt body. In the North Sea Central Graben Zechstein salt there are thick bands of bischofite and carnallite, the last is shown in figure 4 to have a much higher creep rate than halite.

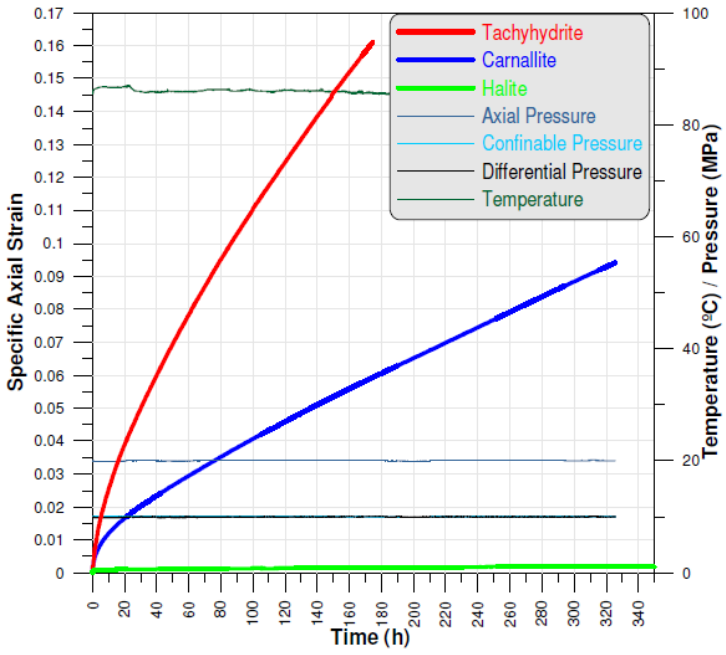

Figure 4: Creep rates for tachyhydrite, carnallite and halite with a temperature of 86ºC and σo = 10 MPa (Costa et al. 2010).

2.2.3. Temperature conductivity

As explained in section 1.1.2, salt creep is greatly impacted by temperature. Higher temperatures causes the salt to be more mobile, which can be a problem when drilling in salt. The temperature effect on creep can be seen in equation 1.
The thermal conductivity, *k*, of salt is 2 -3 times higher than for shale, limestone and sandstone. Salt can then dissipate differences in temperature faster. The creep rate will, depending on the Arrhenius thermal activation term form equation 1, increase by a factor of two when the temperature increases by 16-18^{o}C. Temperature gradients in salt will depend on where in the world the salt is. The temperature gradient for a well drilled in the Butch field, in the North Sea, found to be 4,1^{o}C/100 m (Russell Bulman, personal communication, February15, 2015). Dusseault et al. (2004b) reported findings of temperature gradients up to 3,8^{0}C/100m in the North Sea.

This temperature conductivity is not only a bad thing. When mud is circulated through the borehole, it will in the lower parts of the salt interval cool the salt and thereby reduce the creep rate. In the top salt interval the salt will be heated. This can therefore lead to a more uniform and reliable creep rate across the entire section.
Temperature also has a big impact on the solubility of salt, a balance between the desire to control creep rates and solubility has to be found.

2.2.4. Solubility

Different types of salt will have varying solubility. Solubility is strongly dependent upon temperature, content of the material to be dissolved in the fluid and the nature of the solute. When drilling through salt it is expected that the driller will encounter different types of salt and non-salt inclusions. When these different salts and non-salts are encountered problems can arise if the mud used is not saturated with them. If encountered and the mud is not saturated, these zones will be dissolved, which might create hole enlargement issues (Dusseault et al. 2004b).

In the North Sea Zechstein salt where thick bands of bischofite and carnallite are encountered, the mud has to be saturated with respect to these salts. The general strategy is to saturate the water phase with the most soluble salt to be encountered, NaCl is used in the Gulf of Mexico and KCl-$MgCl_2$ in the North Sea. Water based mud at surface conditions which is saturated

with salt will not be saturated at downhole conditions. North Sea operators have successfully heated the mud in order to create a more uniform downhole circulating temperature in order to avoid washouts (Dusseault et al. 2004b).

A practical method of keeping an equilibrium between solubility and borehole closure is to maintain a balance between creep and salt dissolution. This can be done by using the most appropriate mud type and by isolating shallower formations with a string of casing (Zhong et al. 2008).Fig. 4 shows the relationship between wellbore enlargement and total mud salinity for a 12 ¼" wellbore drilled in the Tahe oilfield.

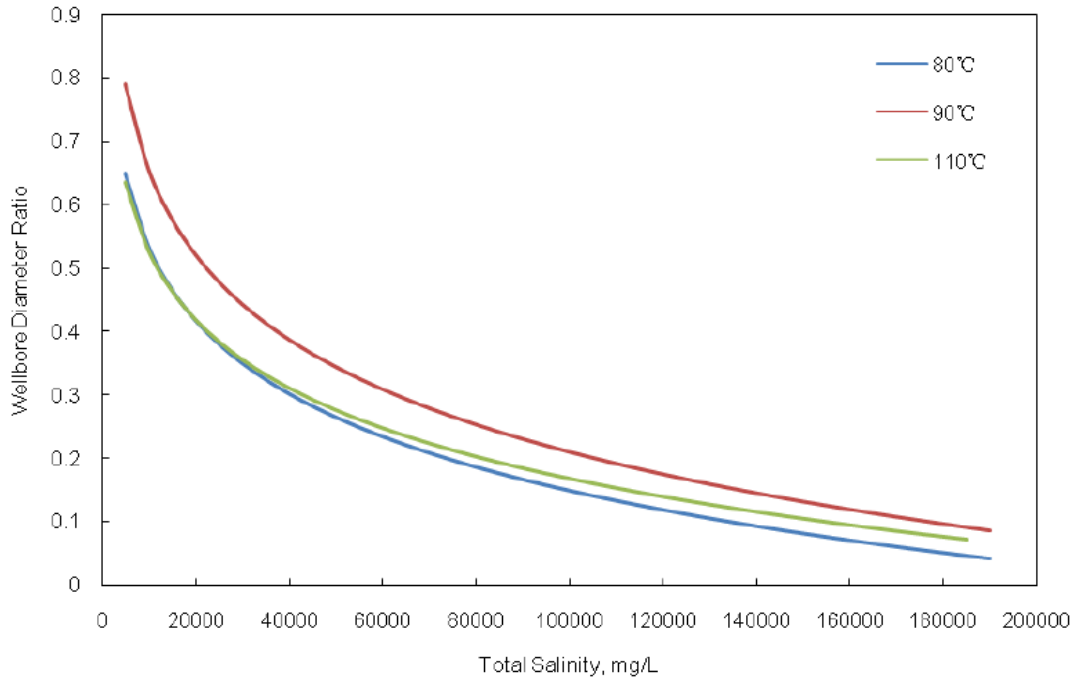

Figure 5: Wellbore diameter ratio vs total salinity for different temperatures, Tahe oilfield (Zhong et al. 2008).

2.3. Salt domes: geometry, growth methods and tectonic regimes

Salt tectonics and halokinesis are the two terms used to describe any movement that significantly influences the type, geometry, localization and / or extent of deformation of a salt body. In simpler terms, they describe the subsurface movement of salt and the formation of subsurface salt structures. Diapirs is a broadly used term within salt tectonics, used to describe a body of salt, which has moved vertically upwards and intrudes the overlying sediments. Although it in strict terms refers to structures that have pierced the overburden, it is often used for other salt structures as well (Fossen 2010, 390).

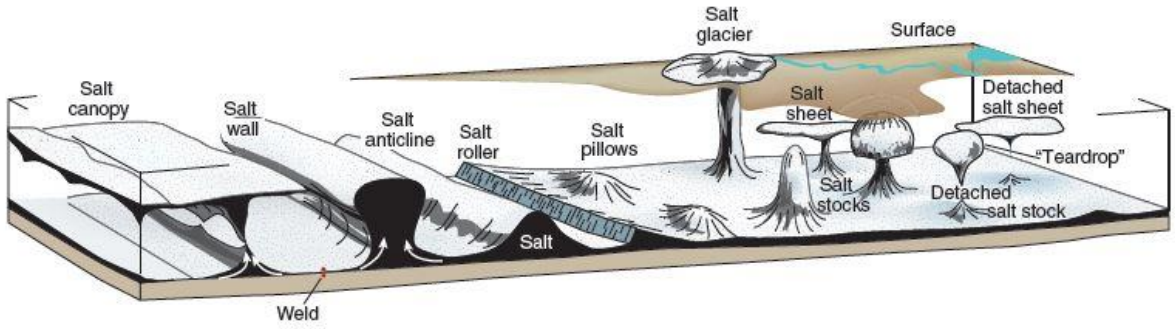

Figure 6: Overview of salt structures (Fossen 2010, 392).

In figure 6 an overview of some salt structures is illustrated. The spatial and temporal controls on the development of various salt bodies will be presented in subsequent subchapters along with a rough presentation of the geometries associated.

2.3.1. Regimes facilitating salt growth

It is unlikely that diapirism can occur without tectonic faulting or fracturing. Once the overburden strata has been weakened salt starts flowing by buoyancy forces. There are three main regimes, extensional, contractional and strike-slip. These regimes will in some places work at different times during the diapir's life, creating different structures.

Extensional regimes

In an extensional regime normal faults cause an extension of the crust. Smaller faults may be regarded as extensional if their horizontal displacement extends the reference layer, regardless of the orientation of the layering (Fossen 2010, 334). Extension of the crust can result from a variety of different faults, from normal faults to horst-and-graben systems, to domino systems. The angles of the faults vary from vertical to horizontal. If the stretching of the crust is extended far enough, passive margins can be established on each side of the continental rift. This is the case for the Viking Graben in the northern parts of the North Sea. Passive margins are also found in areas of the Gulf of Mexico and of the coast of West Africa (Fossen 2010, 347).

As can be understood an extensional regime is a host for many different and complex faulting systems. Some examples are rifting which is created by tectonic forces and gravity driven fault movement creating extensional fault systems because of weak layers, such as salt or clay.

Throughout the literature extensional regimes are thought to be the main initiating factor for the development of diapirism, as argued by Fossen (2010) and Dusseault et al. (2004).

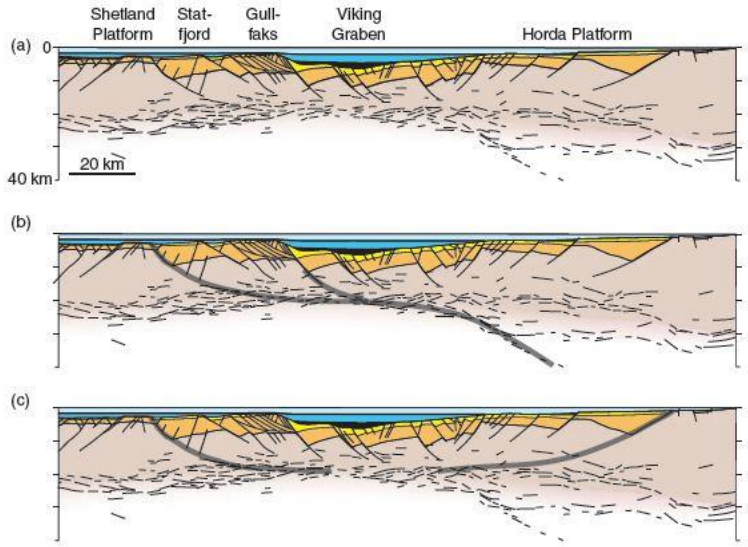

Figure 7: Cross section basen o a deep seismic line across the North Sea, showing varying extensional faulting (Fossen 2010, 345)

Contractional regimes

Contractional deformation forms when tectonic or gravitational forces shorten rocks. It is found in collision zones and in the toe of gravitationally unstable sliding deltas and continental-margin sediments which rests on a weak layer of mud or salt. As long as the surface is used as a reference contractional faults are exclusively reverse faults and thrust faults. Reverse faults have angles steeper than 30^{o} , whilst thrust faults have lower angles (Fossen 2010, 312).

Diapirs that have developed within a contractional regime have often been initiated a result of extension. Contraction can help generate tear drop diapirs or salt sheets, such as salt glaciers (Fossen 2010, 388).

Strike-slip regime

Strike-slip faults are faults where the displacement vector is parallel to the strike of the fault. Strike-slip faults are often steeper than other faults and many will appear as straight structures in map view (Fossen 2010, 356). Famous strike-slip faults are the San Andreas Fault in California and the North Anatolian Fault in Turkey.

Transfer faults are strike-slip faults that transfer displacement from one fault to another. The term is used for strike-slip faults whose tips terminates against other faults or extension fractures, and is therefore bounded (Fossen 2010, 356). Transfer faults can connect half-

grabens with opposite polarity, such as in the East African rift system, the North Sea rift and the Rio Grande rift (Fossen 2010, 357).

Reactive diapirism in strike-slip system tends to occur in releasing stepovers. Salt diapirs in releasing stepovers develop much like in a regional extension illustrated in figure 7 (Fossen 2010, 386).

2.3.2. Growth mechanisms

Salt will not move unless there is a gravitational or mechanical anomaly present (Fossen 2010). The two main activation modes, when discussing salt diapirs, are differential loading and buoyancy as a result of density differences. Differential loading is related to lateral variations in the state of stress created, such as when one area is heavier than another. This mechanism does not require the salt to be at great depths, which would make it an active mechanism in areas such as passive margins or in contractional regimes.
The buoyancy effect comes into play when the salt is buried at great depths and the specific gravity of the salt is lower than that of the surrounding formations. Salt at depths will have a density of around 2.16 g/cm^3, whilst the surrounding formations might have densities ranging from 2.3 g/cm^3 to 2.6 g/cm^3.
With this being said, there will be no activation unless the overburden is somehow weakened, usually through extension as presented in the former subchapter. Diapir initiation or late stage re-activation by overburden removal should also be considered as a growth mechanism for diapirs.

Diapirism is a process of different types of growth. The geometry of a salt dome is greatly dependent upon the timing of when external forces began and ceased to exert their influence, and the regime in which it was built. Figure. 7 illustrates how a typical process for diapirism might, develop in an extensional setting.

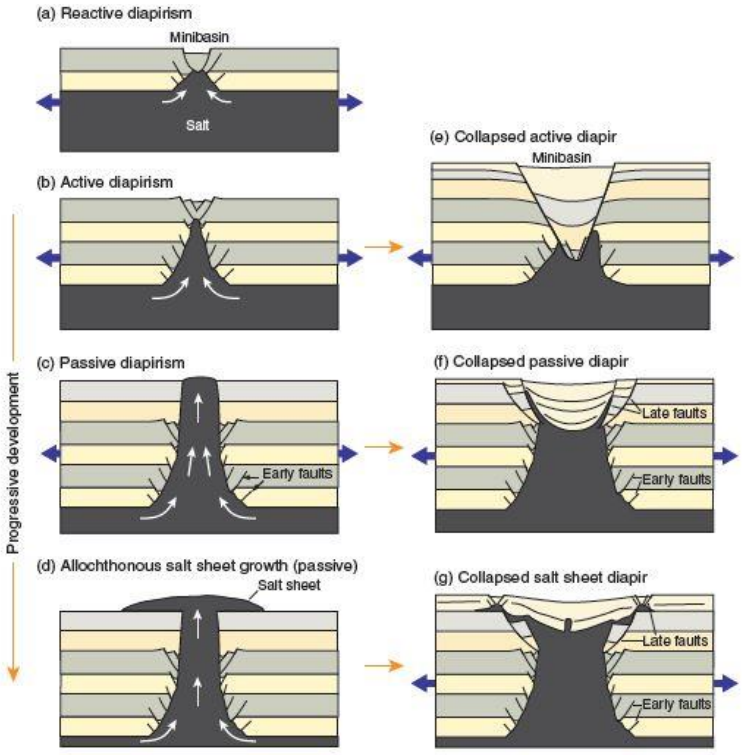

Figure 8: Possible progression of salt diapirism (Fossen 2010, 384).

As explained, in order for salt growth to commence the roof must be weakened. This will induce the reactive diapirism stage. After growth has been initiated active diapirism can take place with salt forcing its way upwards by either buoyancy forces or differential loading or both. At one point salt might rise at a similar rate as the sedimentation, which is known as passive diapirism. If the sediments subside and compact during this stage it is commonly said that the salt diaper is downbuilding. When the rise rate is less than the sedimentation rate during downbuilding the diapir will take an upward-narrowing shape, which is the structure for the Butch Field in the North Sea illustrated in figure 8. When the vertical forces finally overcome the growth forces in the diapir it might be easier for the salt to grow laterally. The salt dome can collapse if the forces supporting it up becomes lower that the overburden pressure.

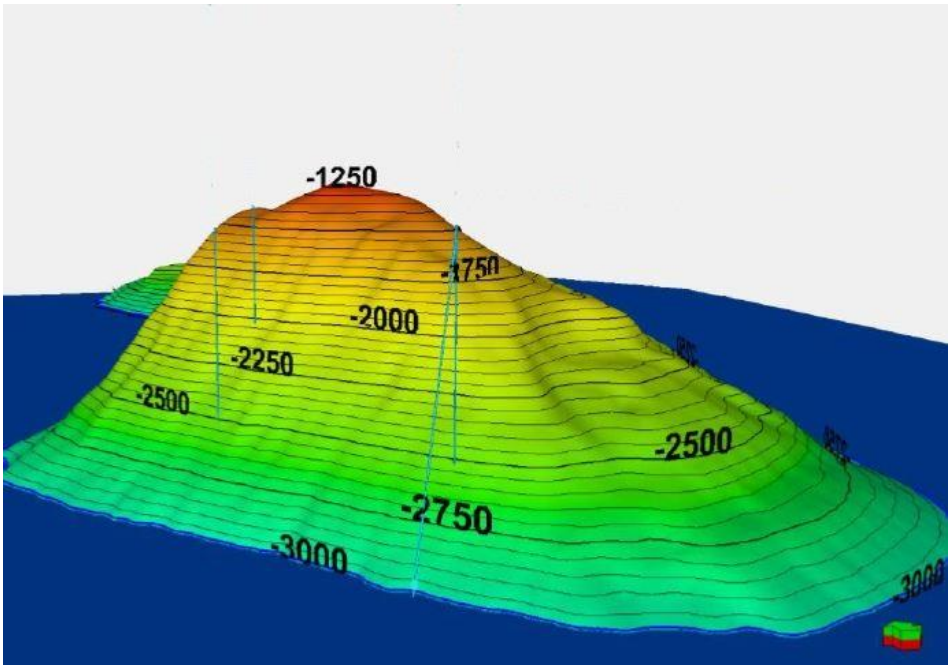

Figure 9: Butch field salt dome, most likely created by downbuilding where the rate of sedimentation was faster than the salt growth rate. Figure provided by Centrica Energi (Valencia et al. 2012).

2.3.3. Geometry

Salt domes can adopt a wide range of geometries, as shown in figure 6. The ultimate morphology of a salt structure is directly related to its mineralogy and the structural setting of the surrounding area. The diapir illustrated in Figure 8 is typical of a salt structure developed in an extensional setting.

Salt structures associated with a contractional regime include tear drop shapes, where the diapir has been subject to lateral forces and has become partly or totally detached from the underlying salt layer. A totally detached body of salt may be less buoyant than the surrounding sediments and could flow laterally, producing an isolated sheet. These structures are invariably evolved from diapirs which have originated under an extensional regime.

What shape a salt structure gets is largely a factor of the salt and the regimes diapirism as occurred in. For a purely extensional regime a diaper like the one in figure 9 is one typical shape, or like the one in figure 8 c). In a contractional regime typical shapes are tear drop diapirs where a former diaper has experienced squeezing. Another typical result of a contractional regime is salt sheets. It should be noted that for shapes like the tear drop diapir, diapirism first occurred in an extensional regime.

3. Salt domes and stress regimes

In the subsurface, the stress state is described by three principal stresses, σ_v, σ_H and σ_h. These three stresses describe the main stress regimes encountered underground. The vertical stress is given by (Fjær et al. 2008):

$$\sigma_v = \int_0^D \rho_f(z) g dz \tag{15}$$

Where $\rho_f(z)$ is the density for each formation encountered on the way down, and z is pointed downwards.

Horizontal stresses will be different from the vertical stress because of the rock's ability to resist shear stresses (Fjær et al. 2008). The horizontal stresses are not so easy to calculate although some correlations with the vertical stress exist. Breckels and van Eekelen found some relations for the smallest horizontal stress which were developed from fracture data in the Gulf of Mexico. The equations can to a certain degree be used in tectonically relaxed areas like GoM and the North Sea (Fjær et al. 2008).
In most of the world horizontal stress anisotropy exists as a result of tectonic stresses, resulting in the development of maximum and minimum horizontal stresses.

The horizontal stresses are difficult to determine by mathematical models and should therefore be determined empirically through tests such as a leak-off-test. This will give both the direction and magnitude of the minimum horizontal stress, and since σ_H is perpendicular its direction can to a certain degree also be determined.

$\sigma_v < \sigma_H < \sigma_h$	Normal fault
$\sigma_H < \sigma_v < \sigma_h$	Strike-slip fault
$\sigma_h < \sigma_H < \sigma_v$	Thrust fault

Table 2: Common faults and their stress states.

With this in mind the stress regimes surrounding various salt structures from around the world will be investigated.

3.1. Stress regimes associated with salt structure geometry

Figure 18 is an example of the general stress regimes found in association with diapirs. The figure shows how the diapir has affected the principal stresses in the surrounding environment. The structure of the dome will have an impact on the stresses and faulting, and the lateral extent of these anomalies. Friedrich et al. (2003) stated that the geometry of the salt body will have a substantial effect on the qualitative character of the stress perturbations. This claim will be discussed in this chapter by using existing literature and field reports. The goal is then to both answer if the geometry has an effect on the stress regimes around salt structures and just how substantial this effect is.

3.1.1. Stress regimes found around diapirs, domes

This subchapter will consider the stress perturbations associated with diapirs and bodies of similar geometry. By reviewing research articles and field reports it can be discussed how generalized stress regimes would develop in the area adjacent to a diapiric structure.

Salt has an inability to sustain differential stresses, it has a need to reach an isotropic condition, meaning that $\sigma_H = \sigma_v$. This inability and constant deformation within the salt will influence the stresses in the formations adjacent to the salt. The principal of stress re-distribution has been investigated by Friedrich et al. (2003), Sanz and Dasari (2010) and others. Both of the mentioned articles studied the stress perturbations around a sphere enclosed in a formation, and Sanz and Dasari also investigated the effect of changing the shape of the sphere to ellipsoids. Through modeling these idealized geometries they got some interesting results regarding how stresses were re-distributed around them. For a perfect sphere the vertical and horizontal stresses above and below were decreased, whilst in the adjacent formations the horizontal stress was increased (Fredrich et al. 2003). This was further discussed by Sanz and Dasari (2010) whose model showed, for a far field stress factor $k = 0,7$, that a 20% reduction of vertical stresses within the salt was the cause for an increase of about 25% in the vertical stresses laterally adjacent to the sphere. For this idealized case it was found that the radius of the sphere is a scaling factor, meaning that the normalized results are the same regardless of the radius (Sanz and Dasari 2010). The stress-arching that occurs around a salt body is similar in character to that which develops in the overburden when pore pressure drawdown of compactable reservoirs occurs during production (Fredrich et al. 2003).

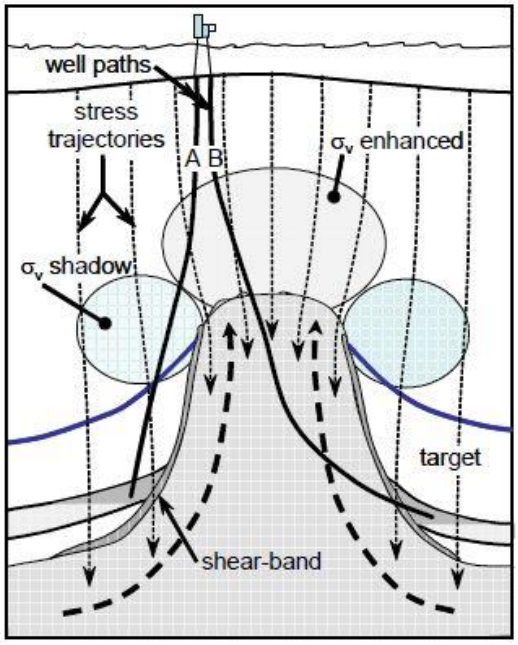

Figure 10: Stress trajectories (Dusseault et al. 2004a).

Sanz and Dasari (2010) took the investigations done by Friedrich et al. (2003) further and introduced elliptically shaped salt bodies. Figure 11 shows the result that the salt pressure is bounded by the *k* factor and 1, from their simulations.

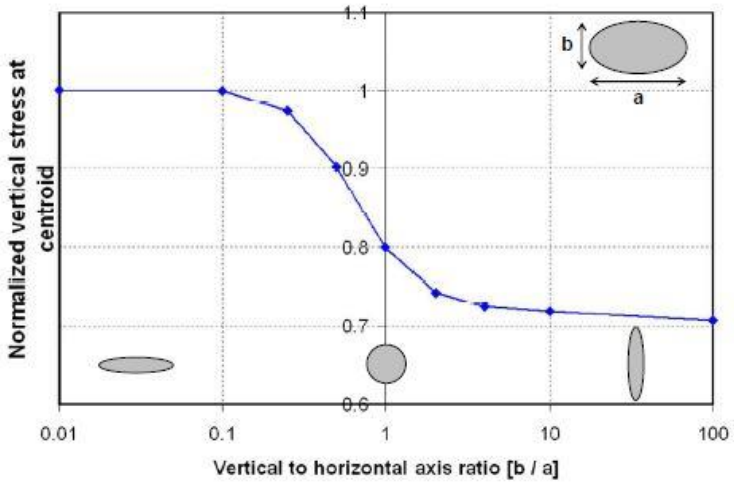

Figure 11: Normalized vertical stress depending on horizontal axis ratio(Sanz and Dasari 2010).

The near horizontal ellipsoid is found to transfer the overburden load through the salt, rather than around it, although the vertical stress then will not change from the far field value there are still significant perturbations of the vertical adjacent to the salt body. For a near vertical ellipsoid the horizontal stresses in the salt remain nearly unchanged and the vertical stress will differ significantly from the far field values (Sanz and Dasari 2010).

Furthermore Sanz and Dasari (2010) investigated whether the connection to the salt source

would have any implications on the type and magnitude of the stress perturbations near the salt. It was found that these perturbations were significantly different from one another. The connected diapir was similar to the horizontal ellipsoid in the fact that the salt in both cases was pressurized by the overburden and itself. The disconnected diapir exhibited a decrease in the vertical stress within the salt body and an increase in the immediately adjacent sediments (Sanz and Dasari 2010). The disconnected diapir can be compared to a teardrop salt body, whilst the connected diapir is similar to the structure presented in fig.9. Stress perturbations around connected diapirs can be significantly greater than in those that are detached.

Re-distribution and increase/decrease in stress values can also be shown in simulations based on actual diapirs modeled in different 3D simulators. Koupriantchik et.al (2005) numerically modeled the stress state around the Munta salt diapir in the Officer Basin of South Australia. By the use of FLAC3D they first created a sphere, as Friedrich et al. (2003) and Sanz and Dasari (2010), which was used to confirm that they could assign typical values to the elastic properties of rock and salt. There are significant stress perturbations close to the Munta diapir; their severity depends on the depth and location. It was argued that some zones of high shear stress showed 50% higher von Mises stress, compared to the far-field values (Koupriantchik et al. 2005). Sanz and Dasari (2010) found in their simulations that the normalized von Mises stress was 70% greater at the salt-sediment interface, although note that this was the result for a perfect sphere. Friedrich et al. (2003) found that the von Mises stress was 50% higher. The distribution of mean and minimum principal stresses are associated with pooling of hydrocarbons, which are assumed to migrate to areas of low mean or minimum principal stress (Koupriantchik et al. 2005).

Another study conducted by Geomechanics Technologies and Subsurface AS for Centrica Energi on the Butch field of the central North Sea, shows somewhat similar trends as for the Munta Diapir in Australia and other studies as presented earlier. It is worth noting that Geomechanics Technologies and Subsurface AS used several different formation layers in their modeling.

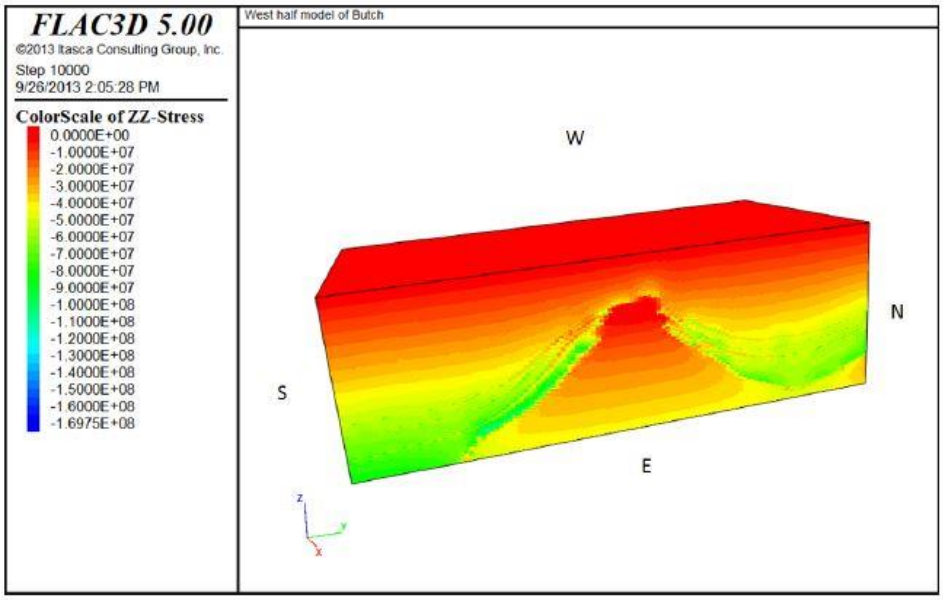

Figure 12: In-situ vertical stress for west half of Butch Field (Geomechanics Technologies 2013).

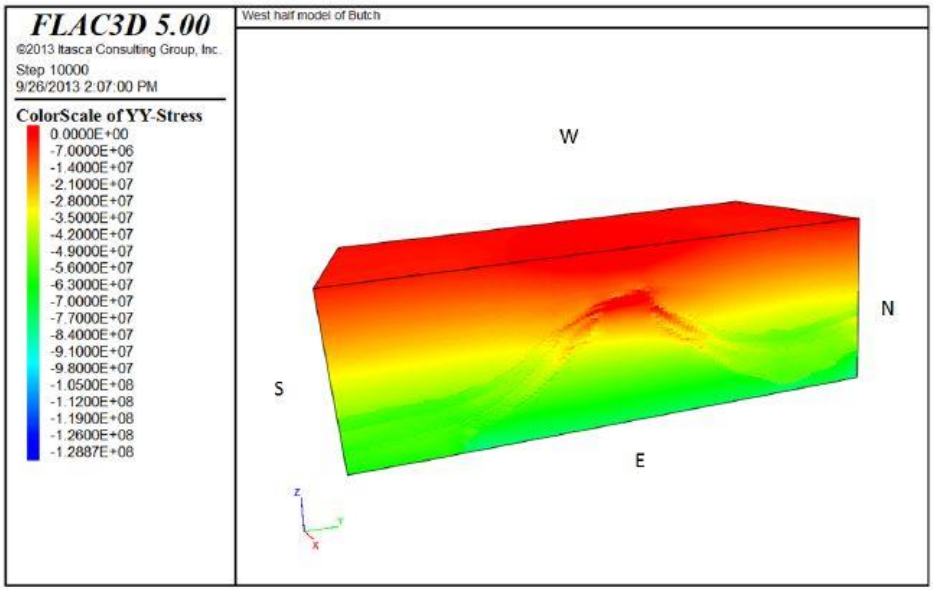

Figure 13: Horizontal stress in N-S direction for west half of Butch Field (Geomechanics Technologies 2013).

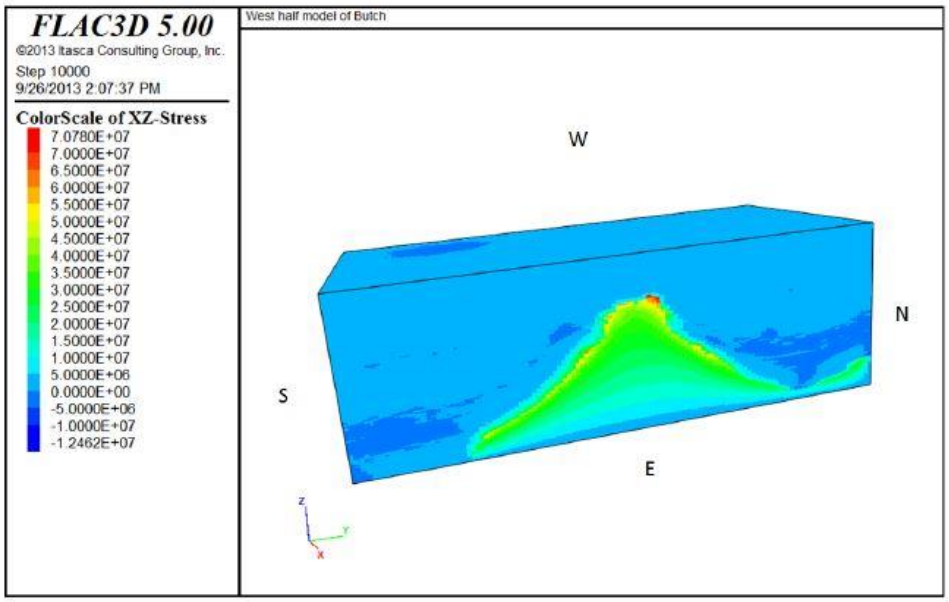

Figure 14: Contour plot of shear stress in xz-direction for west half of Butch Field (Geomechanics Technologies 2013).

Friedrich et al. (2003) deduced that spheroidal or bulbous salt bodies would have a larger impact on the stress state of the surrounding formations. This prediction is, to an extent, proven in the paper by Sanz and Dasari (2010). It was shown that for a connected diapir the stress initialization was not relevant since salt pressure is constrained by the overburden and itself. For a disconnected body the stress initialization was relevant and has to be taken into account as salt pressure can be decoupled from far-field stresses by varying it. The difference between connected versus disconnected is also shown when the normalized vertical stress was compared for varying density contrasts for disconnected and connected diapirs. Figure 15 shows that in the disconnected case, the vertical stress will always be larger adjacent to the salt body, whilst for the connected salt body the vertical stress is less when the overburden sediments are denser than the salt and higher when the salt is denser (Sanz and Dasari 2010).

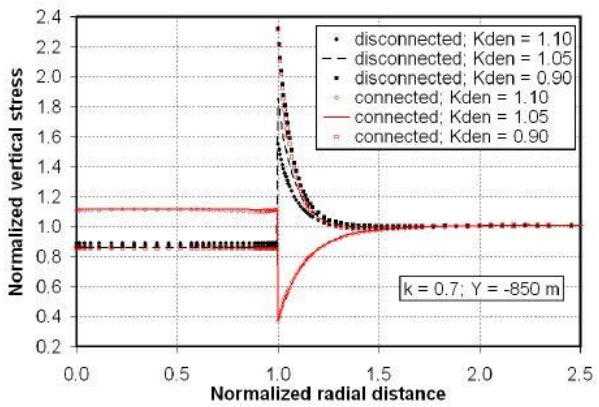

Figure 15: Normalized vertical stresses for different density contrasts (on the flank of the model) (Sanz and Dasari 2010).

As seen from figure 12, there is an increase in the vertical stress adjacent to the diapir. This would indicate, if the results by Sanz and Dasari (2010) holds true, that the salt density in the upper section of the diapir is greater than the sediment density for the Butch field. In a well drilled by Centrica it was found that the upper 20 m of the salt is anhydrite with a density of 2.96 SG. The underlying Halite has a density of 2.03 SG. The average density of the overlying formation for the upper part of the salt is 2.53 SG, which would confirm the results found by Sanz and Dasari (Russell Bulman, personal communication, February15, 2015).

Because of the stress changes in the vicinity of the salt body the stresses are likely to have been re-oriented. The rotation can in some places be as high as 15^{o} around a perfect sphere(Fredrich et al. 2003). It is thought that on the flanks the principal stress direction is horizontal and positioned radially outwards from the salt body, $\sigma_1 = \sigma_r = \sigma_{HMAX}$. The minimum principal stress is thought to be $\sigma_3 = \sigma_\theta = \sigma_{hmin}$, because of the extensional circumferential strain (Dusseault et al. 2004a). This assumption is supported by Nikolinakou et al. (2013) whom by forward modeling diapir evolution found the maximum principal stresses to be perpendicular to the salt face. σ_{HMAX} was found to be the largest closer to the top and σ_{hmin} was in the circumferential (hoop) direction (Nikolinakou, Flemings, and Hudec 2013).

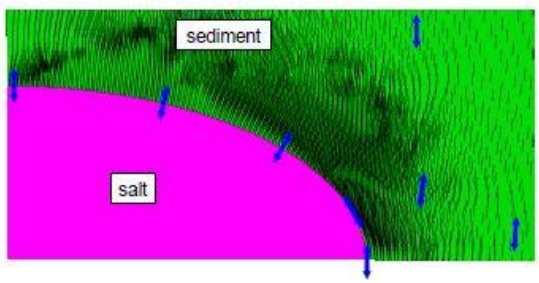

Figure 16: Orientation of most compressive principal stresses outside a elipsoid, b/a =0,5 and far field stress factor k=0,7 (Sanz and Dasari 2010).

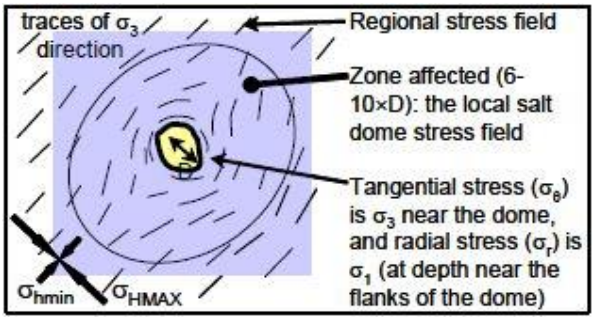

Figure 17: Stress field around a diapir(Dusseault et al. 2004a).

Dusseault et al. (2004a) produced figure 18, showing the generalized stress regimes around a dome. It supports the results found by Sanz and Dasari (2010) that there is a decrease in the vertical stress adjacent to the salt body. Horizontal stresses are predicted to be greater than the vertical stress with increased proximity to the strike-slip and thrust fault areas. This is also in line with the findings of increased horizontal stresses adjacent to salt bodies, as noted in the research papers quoted above and also in the cases based on real salt structures in the North

Sea and Australia. Fracture patterns seen in the Gulf of Mexico and the North Sea also indicate that the fault arrays depicted in Figure 17 are close to reality.
How far the disturbances reach will be a function of form and geometry. Dusseault et al. (2004a) argues that for a radial distance of several times the salt dome diameter in all directions the stress orientations and relative magnitude have been affected by displacement associated with the dome. Sanz and Dasari (2010) have results that would indicate minimal perturbations at 1 times the width of a sphere and approximately 0,5 times the width of a diapir, illustrated in figure 15. For the Butch field in the North Sea stress disturbances extend about 1 km from the edges of the structure (Geomechanics Technologies 2013).

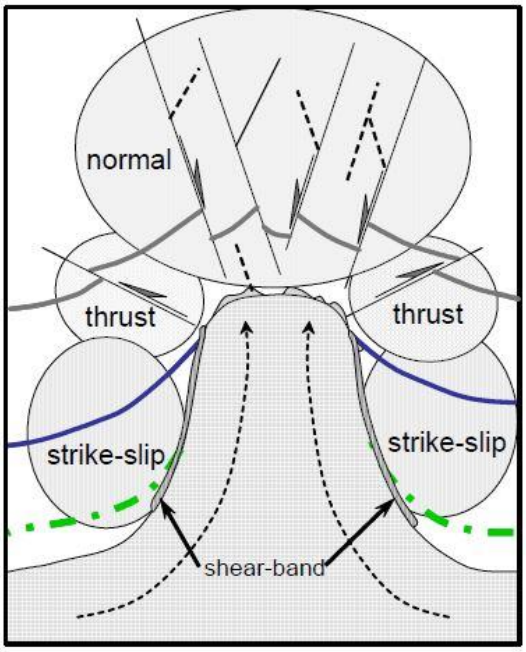

Figure 18: Generalized stress regimes around a salt dome (Dusseault et al. 2004a).

The conclusions so far will then be:

- The inability of salts to sustain differential stresses will influence the stresses adjacent to the salt body.
- The geometry of the salt body will have a great effect to how the stresses will be distributed around the salt body. Horizontal ellipsoids will transfer the vertical stress through its body, whilst the vertical ellipsoid will divert the vertical stresses. Connected diapirs will, like horizontal ellipsoids, transfer the weight of the overburden through the salt body. Stress perturbations around connected diapirs are significantly greater than those adjacent to disconnected salt bodies.
- Stress arching can be compared to that of production induced compaction.

- The Von Mises stresses near a diapir are seen to increase by as much as 50-70%, and should be taken into consideration during wellbore stability calculations.
- The density contrast between sediments and the salt might have an implication in the magnitude of the vertical stresses adjacent to the salt.
- Figure 18 is a good representation of the generalized stress regimes which can develop around a salt dome, based on current literature and on faulting patterns seen in the Gulf of Mexico and the North Sea. This figure can be used as a basis upon which to characterize the stress regimes in real cases.

3.1.2. Stress regimes found around salt sheets and tongues

Allochthonous salt is defined as a sheet like body overlying younger strata. It is a broader term incorporating salt sheet and tongue like geometries. Figure 7 a)-d) shows an example of how salt sheets could form. In a listric environment, rising diapirs will "sense" that $\sigma_v > \sigma_h$ and find it easier to flow horizontally. Around the décollement zone there must be a region of $\sigma_v < \sigma_h$ (Dusseault et al. 2004a). According to a talk by Martin Jackson on the subject of allochthonous salt sheets , there are 35 basins around the world that have this salt geometry(GeologicalSociety 2013). In this report, examples will be from the Gulf of Mexico, as it is one of the most extensively researched areas in the world with salt sheets.

Friedrich et al. (2003) presented results from a perfectly flat modeled deep, extensive salt sheet. Within the sheet the vertical stress is not perturbed from the far-field lithostatic value, but at the edges it is slightly increased. The horizontal stress is reduced above and below, but within the salt the horizontal stress is equal to the lithostatic stress. Horizontal stress difference of up to 35% from the far field value was found adjacent to the salt body for sheet thicknesses of 2500 and 5000m. Because of the decrease in horizontal stress above and below, as compared to vertical stress, the von Mises stress will be elevated here. Spheroidal or bulbous salt bodies are predicted to cause more significant stress perturbations than two dimensional geometries like salt sheets (Fredrich et al. 2003).
Sanz and Dasari (2010) modeled ellipsoids and found results similar to that of Friedrich et al. (2003). It was found that the vertical stress was the same as the far-field value, meaning it was easier to transfer the overburden through the salt body, when the horizontal extent was big enough. Compared to Friedrich et al. (2003) who only reported slightly increased vertical

stresses adjacent to the salt sheet, Sanz and Dasari (2010) report significant perturbations in the same area. As with diapirs, the isotropic stress state in the salt change both the orientation and magnitudes of stresses in the sediments close to them. Principal stresses become normal and parallel to the salt sediment interface (Sanz and Dasari 2010).

Allochthonous salt sheets are often of a complex geometrical nature. The idealized flat salt sheet gives insight into how the salt reaches an isotropic state, which might help in understanding how stress perturbations around more complex geometries arise.

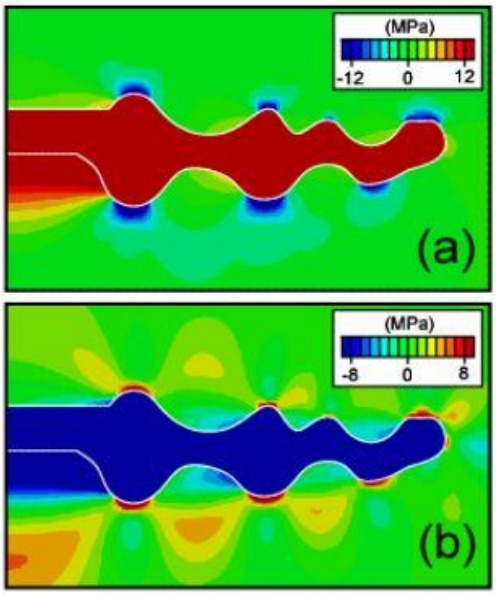

Figure 19: Stress perturbations are from salt relaxation around an irregular salt sheet a) Changes of minimum principal stress and b) changes of von Mises Stress (Luo et al. 2012).

Figure 19 shows an irregular salt sheet from a study done by Luo et al. (2012) on the near-salt stresses and wellbore stability for different geometries. The convex curves shows a decrease of the minimum principal stress, and a concentration of the von Mises stress. The concave curves shows an increase of the minimum principal stress and a decrease of von Mises stress. It also shows how much the convex curves affect the sediments above and below the concave curves. For the case in figure 19 no plasticity has been added into the sediments in the finite-element model, the added plasticity would moderate the results (Luo et al. 2012).

The Mad Dog salt is located in the Green Canyon in the Gulf of Mexico, and is a part of the larger Sigsbee salt canopy. Nikolinakou et al. (2013) built a two dimensional finite-element model of this field and got some interesting results. It should be noted that this article is written by the same authors of the article mentioned in the previous paragraph.
The Mad Dog salt is 20 km long and 0,1-4 km high. Because of the significant length of the

salt body, sections with comparable horizontal to vertical dimensions converge to an isostatic value between the overburden value and the initial horizontal stresses (Nikolinakou et al. 2013). This is in line with the results from Friedrich et al. (2003) and Sanz and Dasari (2010). Horizontal stresses within the salt body will then be greater than that of the sediments surrounding it. The salt will therefore create a horizontal loading on the wall rocks in basins, which again will lead to an increase in lateral stress. The increase in horizontal stress, presented in figure 20, leads to a decrease in shear stress. That would explain the results the authors got in their previous article presented in figure 19.

Adachi et al (2012) made a 3D finite-element model covering more than 10 blocks also located in Green Canyon of the Gulf of Mexico. Convex geometries of the salt in this study showed low values of "mud weight window" as the minimum principal stress was low, and the concave showed high values of "mud weight window" as the fracture gradient was high (Adachi et al. 2012). This supports the findings by Luo et al. (2012) and Nikolinakou et al. (2013).

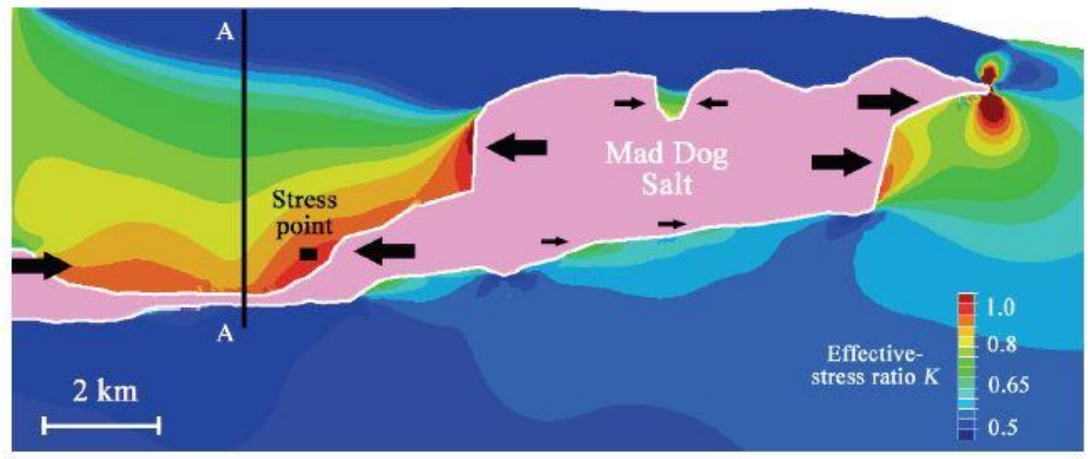

Figure 20: The effective stress ratio K = σ'$_h$/σ'$_v$, in the wall rocks of the Mad Dog salt (Nikolinakou et al. 2013).

Nagy et al. (2013) results on mud weight windows for a complex structure in the Gulf of Mexico shows the same trend of high mud weight window in the concave areas of the salt and low mud weight windows at the convex areas (Nagy et al. 2013). The horizontal loading predicted by Luo et al. (2013) can be transferred to salt tongue geometries.

Friedrich et al. (2007) made a 3D model for two different seismic lines in the Spa prospect, Walker Ridge 285 # 1, in the Gulf of Mexico. It was found that at the relative flat bottom there was a reduction of the von Mises stress at most of the bottom of the salt. This would indicate elevated minimum principal stress below the salt. It was found that at locations of lower mean stress, which was where the minimum horizontal stress was reduced, was also the

areas where the von Mises stress was elevated. These areas were at convex heights in the salt (Fredrich et al. 2007). Since the geometry is not well defined in their study, the results are also uncertain.

Van Der Zee, Taylor and Brudy (2012) presented a workflow for creating a realistic 3D finite-element based geomechanical simulations. As the rest of the literature, they also report reduced minimum principal stress and stress ratio at a convex salt-clastic interface, and the same values increased at concave salt-clastic interface. They found that their calculated values had an error less than 5 % from measured data (Van Der Zee, Taylor, and Brudy 2012).

Inclined salt will dominate the interaction between salt and sediments. From the literature presented above, the geometry of the allochthonous salt sheet is important in order to predict stress perturbations. Flat geometry leads to barely any perturbations, whilst concave and convex salt-sediment interfaces have the potential to create significant perturbations. The knowledge of where stresses are reduced and increased, will have large implications on drilling operations.

Conclusions for allochthonous salt sheets:

- Flat salt sheets will have vertical and horizontal stresses equal to the far-field lithostatic value in the salt. Above and below the horizontal stress will be reduced. It is expected that there will be significant perturbations in vertical and horizontal stress adjacent to the salt body.
- Often of a complex geometrical nature meaning that salt sections with comparable horizontal to vertical dimensions converge to an isostatic value between the overburden value and the initial horizontal stresses. This will create a horizontal loading on the wall rocks in basins. As for diapirs, the principal stresses will become parallel and normal to the salt-sediment interface.
- Convex curves shows a decrease in the minimum principal stress, and an increase in the von Mises stress.

  Concave curves shows an increase in the minimum principal stress, and a decrease in the von Mises stress.

3.2. General

This section will discuss areas related to the stress perturbations created by both diapirs and allochthonous salt sheets. The discussed topics are affected by the altered stress states and growth of salt.

3.2.1. Regional stress influence

If the stresses induced by diapir growth are influenced by regional stress directions or not, is an interesting question. Dussealt et al. (2004a) wrote that the most recent large tectonic event may have overprinted the previous stress history. In the great majority of cases, it is clear which stress field is dominant. From the literature on stress perturbations induced by salt structures, it is clear that within a certain range these perturbed stresses dominate. The regional stress directions are therefore not thought to be an influencing factor on the stresses induced by diapir growth within a certain range of the diapir in the current stress state.
The focus could, however, be shifted towards the way the regional stresses has affected the growth of the diapir, and therefore also how the stresses were induced by the diapir. In strongly anisotropic horizontal stress cases salt structures should display some elongation normal to the minimum horizontal stress (Dusseault et al. 2004a). This is the case for the Butch field in the North Sea and the Munta diapir in Australia, as presented earlier. Butch field is elongated in the direction of the regional extensional faulting trend, NW-SE (Davison et al. 2000). This is also the direction of the regional maximum horizontal stress.
Regional stresses will be a factor in shaping the salt structure, and therefore also influence the stress distribution induced by diapirs.

3.3. Pore pressure

The interdependence between pore pressure and stress is critical as the safe range of drilling pressures is defined between the minimum principal stress and the wall rock pore pressure (Nikolinakou et al. 2011). There are only a very few studies that have linked pore pressure and stress perturbations together in a single geomechanical model.
The norm for introducing pore pressures into geomechanical models are usually based on the assumption of hydrostatic pressure, on seismic velocities, on actual drilling data or on a combination of these. Pore pressure and stresses are coupled through the effective stress principle and the theory of pressure dissipation (Nikolinakou et al. 2011).

In some cases the assumption of a hydrostatic model might be accurate. Nikolinakou et al. (2011) concludes that salt relaxation, in a model environment, induces an undrained loading.

This is because salt relaxation occurs at least 4 orders of magnitude faster than pore pressure dissipation. Given enough time the pore pressure will revert back to a hydrostatic setting.

As geomechanical models of salt bodies evolve, the introduction of pore pressures is one of the areas that should be put focus on. For practical use, it seems as pore pressures derived from seismic velocities and exploratory wells, gives an adequate estimation of pore pressures.

4. Wellbore stability

4.1. Stresses around boreholes

When drilling a hole into the subsurface, an imbalance will occur around the borehole. Understanding how stresses are distributed around a well is important in order to make sure the hole is stable. This subsection will give a short introduction to the general elastic stresses around a wellbore.

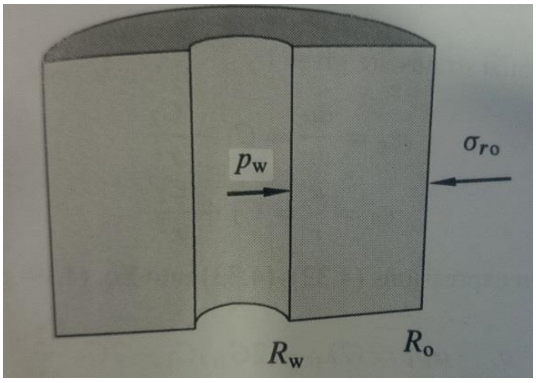

Figure 21: Hollow cylinder model (Fjær et al. 2008, 137).

Wellbores are often deviated, a general solution to the elastic stresses around a wellbore where the horizontal stresses are anisotropic is needed. In order to get to the general solution, a set of transformation formulas are required to move from the global coordinate system to a coordinate system where the z-axis points along the axis of the hole. These are given in appendix A. The general elastic solution at the borehole wall with constant pressure is given as (Fjær et al. 2008, 148):

$$\sigma_r = p_w \tag{16}$$

$$\sigma_\theta = \sigma_x^0 + \sigma_y^0 - 2\left(\sigma_x^0 - \sigma_y^0\right)cos2\theta - 4\tau_{xy}^0 sin2\theta - p_w \tag{17}$$

$$\sigma_z = \sigma_z^0 - \nu_{fr}\left[2\left(\sigma_x^0 - \sigma_y^0\right)cos2\theta + 4\tau_{xy}^0 sin2\theta\right] \tag{18}$$

$$\tau_{r\theta} = 0 \tag{19}$$

$$\tau_{\theta z} = 2\left(-\tau_{xz}^0 sin\theta + \tau_{yz}^0 cos\theta\right) \tag{20}$$

$$\tau_{rz} = 0 \tag{21}$$

σ_x^0, σ_y^0, σ_x^0 , $\tau_{r\theta}^0$, $\tau_{\theta z}^0$, τ_{rz}^0,are the stresses and shear stresses found by utilizing transformation formulas A1-A7 in appendix A. θ is the angle between x and y and p_w is the wellbore pressure.

Equation 16-21 are the solutions for materials with constant pore pressure. If the material in question has varying pore pressure, pore pressure terms can be added, this thanks to the superposition principle.

For more in depth reading on the mathematics behind the presented solutions, the reader is referred to the book Petroleum related rock mechanics 2nd edition by Fjær et al. (2008).

4.2. Failure criterion

There are numerous failure criteria to choose from when investigating the limits for a stable well. In this section some of the most common criteria, for different failure modes is presented.

4.2.1. Tensile failure

Tensile failure occurs when the effective tensile stress across some plane exceeds the tensile strength. When tensile failure occurs the rock will fracture. The theory behind fracking is to increase the well pressure locally until tensile failure occurs.
Tensile failure will occur at the borehole wall if (Fjær et al. 2008, 156):

$$\sigma'_\theta < -T_0 \tag{22}$$

T_0 is the sign for tensile strength.

4.2.2. Shear

High enough shear stress along a plane in the rock will cause shear failure. Morh's hypothesis states that the critical shear stress for which shear failure occurs depends on the normal stress acting on the failure plane. This can be drawn from the known fact that frictional forces that acts against relative movement of two bodies in contact depends on the force that presses the body together (Fjær et al. 2008, 60).
A well-known criterion for shear failure is the Mohr-Coulumb criterion. It is based on the assumption that the function of the normal stress is a linear one. It can be defined as (Fjær et al. 2008, 64):

$$\sigma'_1 = C_0 + \sigma'_3 tan^2\beta \tag{23}$$

σ_1' is the largest effective stress, C_0 is the uniaxial compressive strength, σ_3' is the smallest effective stress and β is the angle for which the failure criteria is achieved.

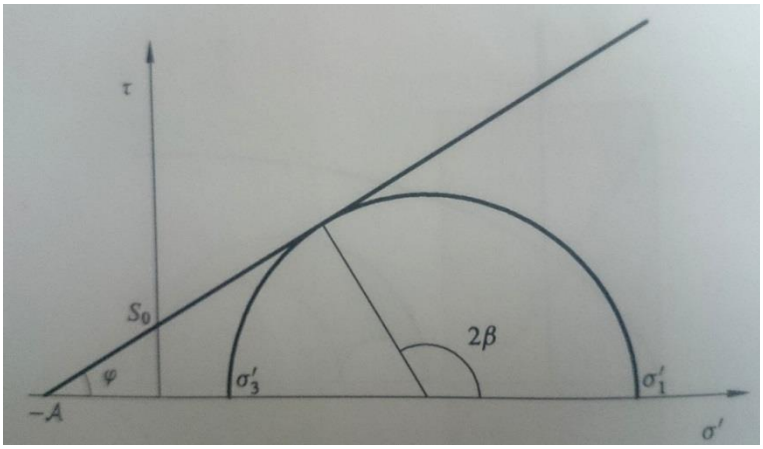

Figure 22: Mohr-Coulumb criterion in the τ-σ' space (Fjær et al. 2008, 62).

Figure 22 shows Mohr-Coulumb criterion in the τ-σ' space. S_0 is the cohesion and φ is the angle of internal friction. The angle of internal friction varies in different rocks; Sandstone has an internal friction angle of about 30^0, Chalk has 10-30^0 and shale has 10-20^0.
The angle of internal friction is related to β (Fjær et al. 2008, 62):

$$\beta = \frac{\pi}{4} + \frac{\varphi}{2} \tag{24}$$

The Mohr-Coulumb criterion given in equation 23 does not account for the intermediate stress. As stresses around a well are 3 dimensional, it is necessary to extend the two dimensional failure criterions.

An often used measure of shear stresses is the von Mises criterion:

$$\sigma_{VM} = \sqrt{\frac{1}{2}[(\sigma_1 - \sigma_2)^2 + (\sigma_1 - \sigma_3)^2 + (\sigma_2 - \sigma_3)^2]} \tag{25}$$

4.2.3. Generalized three dimensional failure criterions

Experimental evidence has shown that the intermediate principal stress has a significant impact on the strength of several rocks (Fjær et al. 2008, 70). Because of the influence of σ_2, several failure criteria has been proposed. The von Mises criterion, as given in equation 25, is one of these criteria. The Drucker-Prager criterion, a generalization of the Mohr-Coulumb criterion, is given as (Belhouchet and Ali 2013):

$$J_2^{1/2} = M\frac{1}{3}(\sigma_i + \sigma_j + \sigma_k) + N \tag{26}$$

Here J_2 is the second invariant of the deviatoric stresses, and M and N are material properties.

$$J_2 = \frac{1}{6}\left[(\sigma_i - \sigma_j)^2 + (\sigma_i - \sigma_k)^2 + (\sigma_k - \sigma_j)^2\right] + \sigma_{ij}^2 + \sigma_{ik}^2 + \sigma_{jk}^2 \tag{27}$$

$$M = \frac{2\sqrt{3}sin\varphi}{3 - sin\varphi}, N = \frac{2\sqrt{3}\ S_0\ cos\varphi}{3 - sin\varphi} \tag{28}$$

φ is the internal friction angle, $\sigma_{ij,ik,jk}$ are the three shear stresses and S_0 is the inherent shear strength, cohesion, of the rock.

The modified Lade criterion is an empirical failure criterion based on observations of the behavior of soils. It seems to account for the influence of the intermediate stress on shear strength in a realistic way, and is therefore a useful criterion for practical calculations (Fjær et al. 2008, 72):

$$\frac{I_1'^3}{I_3'} - 3^3 = \eta_L \tag{29}$$

Here I'_1 and I'_3 modified representations of the first and third invariant.

$$I_1' = (\sigma_1' + S_L) + (\sigma_2' + S_L) + (\sigma_3' + S_L) \tag{30}$$

$$I_3' = (\sigma_1' + S_L)(\sigma_2' + S_L)(\sigma_3' + S_L) \tag{31}$$

$$S_L = \frac{S_0}{tan\varphi} \tag{32}$$

$$\eta_L = 4tan^2\varphi\frac{9 - 7sin\varphi}{1 - sin\varphi} \tag{33}$$

S_L is a material parameter related to cohesion and friction angle, η_L is related to friction angle.

Modified Wiebols and Cook criterion is another criterion which Colmenares and Zoback (2002) recommends to use. They argue that this criterion and the modified Lade criterion will

yield good results in most cases, especially for rocks with strong σ_2-dependence. Both of them will not overestimate the C_0 as much as the Mohr-Coulumb criterion. The modified Wiebols and Cook criterion is given as (Colmenares and Zoback 2002):

$$J_2^{1/2} = A + B\frac{1}{3}(\sigma_1 + \sigma_2 + \sigma_3) + C\left[\frac{1}{3}(\sigma_1 + \sigma_2 + \sigma_3)\right]^2 \quad (34)$$

$$J_2^{1/2} = \sqrt{\frac{1}{6}((\sigma_1 - \sigma_2)^2 + (\sigma_1 - \sigma_3)^2 + (\sigma_2 - \sigma_3)^2)} \quad (35)$$

The parameters A, B and C are determined so that equation 37 is constrained by rock strengths under both triaxial and biaxial conditions (Colmenares and Zoback 2002):

$$C = \frac{\sqrt{27}}{2C_1 + (tan^2\beta - 1)\sigma_3 - C_0} \times \left(\frac{C_1 + (tan^2\beta - 1)\sigma_3 - C_0}{2C_1 + (2tan^2\beta - 1)\sigma_3 - C_0} - \frac{tan^2\beta - 1}{tan^2\beta + 2}\right) \quad (36)$$

$$B = \frac{\sqrt{3}(tan^2\beta - 1)}{tan^2\beta + 2} - \frac{C}{3}(2C_0 + (tan^2\beta + 2)\sigma_3) \quad (37)$$

$$A = \frac{C_0}{\sqrt{3}} - \frac{C_0}{3}B - \frac{C_0^2}{9}C \quad (38)$$

Here $C_1 = (1+0.6\ \tan\varphi)C_0$

Due to the way in situ stresses are altered by the presence of a borehole, and that the stress state is rarely $\sigma_2=\sigma_3$, means that the wellbore is normally under a polyaxial stress state (Zimmerman and Al-Ajmi 2006). Zimmerman and Al-Ajmi proposed the Mogi-Coulomb criterion in 2006:

$$\tau_{oct} = a + b\ \sigma_{m,2} \quad (39)$$

Here τ_{oct} is the shear octahedral stress, $\sigma_{m,2}$ is the mean normal stress in the intermediate principal stress direction, a and b are given as (Zimmerman and Al-Ajmi 2006):

$$a = \frac{2\sqrt{2}}{3}Ccos\varphi, \qquad b = \frac{2\sqrt{2}}{3}\sin\varphi \quad (40)$$

Here C is the uniaxial compressive strenght and φ is the internal friction angle.

The Mogi-Coulomb criterion extends the Mohr-Coulumb into the polyaxial stress domain.

4.2.4. Compaction

High porosity materials with a relatively open structure can experience that its pores collapse and the material packs closer together, this process is called compaction. Pore collapse may occur under pure hydrostatic loading. Fjær et al. (2008) argues that microscopically failure will be because of local excessive shear forces acting through grains and grain contacts. Pore collapse, leading to compaction, can therefore be viewed as distributed shear failure in the material (Fjær et al. 2008). Compaction failure represents the end cap of the failure surface in the principal stress space.

4.2.5. Borehole failure

In this section solutions for maximum and minimum mud weights under different conditions will be presented for the Mohr-Coulomb criterion, the Modified lade criterion and the Mogi-Coulomb criterion.

Interchanging the far-field stresses in equation 16-21 it is possible to get the borehole stresses along any trajectory. As an example for the Mohr-Coulomb criterion a vertical borehole with unequal horizontal stresses will be used (Fjær et al. 2008, 149):

$$\sigma_r = p_w \tag{41}$$

$$\sigma_\theta = \sigma_H + \sigma_h - 2(\sigma_H - \sigma_h)cos2\theta - p_w \tag{42}$$

$$\sigma_z = \sigma_v - \nu_{fr}2(\sigma_H - \sigma_H)cos2\theta \tag{43}$$

$$\tau_{r\theta} = \tau_{rz} = \tau_{\theta z} = 0 \tag{44}$$

θ is relative to the direction of the major horizontal stress, and v_{fr} is the Poisson's ratio.

Putting this into the Mohr-Coulomb criterion and solving for critical well pressure gives:

$\sigma_1 > \sigma_2 > \sigma_3$	Critical well pressure	
$\sigma_\theta > \sigma_z > \sigma_r$	$p_{w,min} = p_f + \frac{3\sigma_H - \sigma_h - 2p_f - C_o}{1 + tan^2\beta}$	(45)
$\sigma_z > \sigma_\theta > \sigma_r$	$p_{w,min} = p_f + \frac{\sigma_v + 2\nu_{fr}(\sigma_H - \sigma_h) - p_f - C_o}{tan^2\beta}$	(46)
$\sigma_z > \sigma_r > \sigma_\theta$	$p_{w,min} = \sigma_h - 3\sigma_H + p_f + \frac{\sigma_v + 2\nu_{fr}(\sigma_H - \sigma_h) - p_f - C_o}{tan^2\beta}$	(47)

Table 3: Critical well pressure for a vertical wellbore using the Mohr-Coulumb criterion.

The fracture pressure according to Mohr-Coulomb is then:

$$p_{w,max}^{frac} = 3\sigma_h - \sigma_H - p_f + T_0 \quad (48)$$

The collapse and fracture pressures for the Mogi-Coulomb criterion is given in figure 23 and 24:

Mogi–Coulomb criterion for collapse pressure in vertical wellbores

Case	$\sigma_1 \geqslant \sigma_2 \geqslant \sigma_3$	Borehole failure will occur if $P_w \leqslant P_{wb}$, where P_{wb} is given by
1	$\sigma_z \geqslant \sigma_\theta \geqslant \sigma_r$	$P_{wb1} = \frac{1}{6-2b'^2}\left[(3A+2b'K) - \sqrt{H+12(K^2+b'AK)}\right]$
2	$\sigma_\theta \geqslant \sigma_z \geqslant \sigma_r$	$P_{wb2} = \frac{1}{2}A - \frac{1}{6}\sqrt{12[a'+b'(A-2P_0)]^2 - 3(A-2B)^2}$
3	$\sigma_\theta \geqslant \sigma_r \geqslant \sigma_z$	$P_{wb3} = \frac{1}{6-2b'^2}\left[(3A-2b'G) - \sqrt{H+12(G^2-b'AG)}\right]$

where
$A = 3\sigma_H - \sigma_h$
$B = \sigma_v + 2\nu(\sigma_H - \sigma_h)$
$H = A^2(4b'^2 - 3) + (B^2 - AB)(4b'^2 - 12)$
$K = a' + b'(B - 2P_0)$
$G = K + b'A$

Figure 23: Mogi-Coulumb criterion for collapse pressure in vertical wellbores. Here a'=2Ccosφ and b'=sinφ (Al-Ajmi and Zimmerman 2006).

Mogi–Coulomb criterion for fracture pressure in vertical wellbores

Case	$\sigma_1 \geqslant \sigma_2 \geqslant \sigma_3$	Borehole failure will occur if $P_w \geqslant P_{wf}$, where P_{wf} is given by
1	$\sigma_z \geqslant \sigma_\theta \geqslant \sigma_z$	$P_{wf1} = \frac{1}{6-2b'^2}\left[(3D+2b'N) + \sqrt{J+12(N^2+b'DN)}\right]$
2	$\sigma_z \geqslant \sigma_z \geqslant \sigma_\theta$	$P_{wf2} = \frac{1}{2}D + \frac{1}{6}\sqrt{12[a'+b'(D-2P_0)]^2 - 3(D2E)^2}$
3	$\sigma_z \geqslant \sigma_z \geqslant \sigma_\theta$	$P_{wf3} = \frac{1}{6-2b'^2}\left[(3D-2b'M) + \sqrt{J+12(M^2-b'DM)}\right]$

where
$D = 3\sigma_h - \sigma_H$
$E = \sigma_v - 2\nu(\sigma_H - \sigma_h)$
$J = D^2(4b'^2 - 3) + (E^2 - DE)(4b'^2 - 12)$
$N = a' + b'(E - 2P_0)$
$M = N + b'D$

Figure 24: Mogi-Coulumb criterion for collapse pressure in vertical wellbores. Here a'=2Ccosφ and b'=sinφ (Al-Ajmi and Zimmerman 2006).

The critical wellbore pressure for any direction using the modified Lade criterion is given by equation 49-56 (Ewy 1999):

$$p_w = \frac{(B - C^{1/2})}{2A} \quad (49)$$

$$A = \sigma_z + S_L - p_p B = A\sigma_{\theta^n} - \tau_{\theta^z}^2 \quad (50)$$

$$B = A\sigma_{\theta^n} - \tau_{\theta^z}^2 \tag{51}$$

$$C = B^2 - 4A\{D - (S_L - p_p)[A(\sigma_{\theta^n} + S_L - p_p) - \tau_{\theta^z}^2]\} \tag{52}$$

$$D = \frac{(\sigma_{\theta^n} - \sigma_z + 3S_L - 3p_p)^3}{27 + \eta_L} \tag{53}$$

$$\sigma_{\theta^n} = \sigma_x + \sigma_y - 2(\sigma_x - \sigma_y)\cos 2\theta - 4\tau_{xy}\sin 2\theta \tag{54}$$

$$\sigma_z = \sigma_{zz} - \mu[2(\sigma_x - \sigma_y)\cos 2\theta - 4\tau_{xy}\sin 2\theta] \tag{55}$$

$$\tau_{\theta^z} = 2[\tau_{yz}\cos\theta - \tau_{zx}\sin\theta] \tag{56}$$

S_L and η_L are found in equations 32 and 33, σ_{zz} acts in the direction of the wellbore.

4.3. Data and assumptions made

This section will present the data and some basic assumptions made for calculating the stability of wellbores at several specific depths.

Table 4 gives the material properties used by GeoMechanics Technologies and Subsurface As during their simulations on the Butch salt structure depicted in figure 9. These numbers will be used for the wellbore stability analysis in this thesis, as the stress data will be gathered from their report. It should be noted that the densities, and the other data, are based on the averages of several wells, some not related to the Butch salt structure, but nearby. This has the potential to give some errors.

	Density (kg/m^3)	**Youngs modulus, E (GPa) (dynamic)**	**Youngs modulus, E (GPa) (static)**	**Static bulk modulus (GPa)**	**Static shear modulus (GPa)**	**Average cohesion (MPa)**	**Average friction angle**
Surface (Claystone)	2010	2,48	1,66	1,84	6,14	3,43	18,93
Hordaland (Claystone)	2140	3,09	2,06	2,29	7,63	3,85	21,08
Balder (Claystones)	2370	5,62	3,75	4,17	1,39	5,21	27,55
Ekofisk (Chalk)	2500	17,7	11,8	10,1	4,52	8	38,7
Rødby (Mudstones)	2560	7,64	5,09	3,69	2,01	5,71	29,72
Mandal (Carbonaceous claystone)	2480	13,6	9,08	5,74	3,67	6,67	33,63
Ula (Sandstone)	2420	14,8	9,9	7	3,91	7,23	35,87
Zechstein (Salt)	2820	8,02	5,34	8,91	1,91	6,57	33,33

Table 4: Material properties part 1, extracted from report on the Butch salt dome by Geomechanics Technologies (Geomechanics Technologies 2013).

Table 5 gives some other material properties not found in the report by GeoMechanics Technologies and Subsurface As. These numbers are from reports by Weatherford and Halliburton. Tensile strength is assumed to be 10% of UCS. PS! These numbers are from well 8/10-4S on the Butch salt dome.

Depth (TVD, m)	UCS (MPa)	Poissons ratio	Tensile Strength (MPa)	Plastic strain index
0-2500	12,5 (6)	0,375	1,25	
2500-2700	32,5(32,5)	0,2/0,3		
2700-2900	20(13)	0,3		
2900-3000	27,5(36)	0,25	2	0,31

Table 5: Material properties part 2, extracted from reports by Weatherford and Halliburton.

The stability analysis is done over 4 depths, for different well paths. The first depth will be above the salt structure, meaning there will be no effect from the salt here. Then three more depths corresponding to the theoretical faulting regimes given by Dussealt et al. (2004a) in fig. 18. The chosen depths are: 500 m, 800 m, 1750 m and 2895, with hole diameters of 17 ½ “, 12 ¼” and 8”. The base case is a vertical well straight down into the reservoir formation, other well paths used are shown in figure 25.

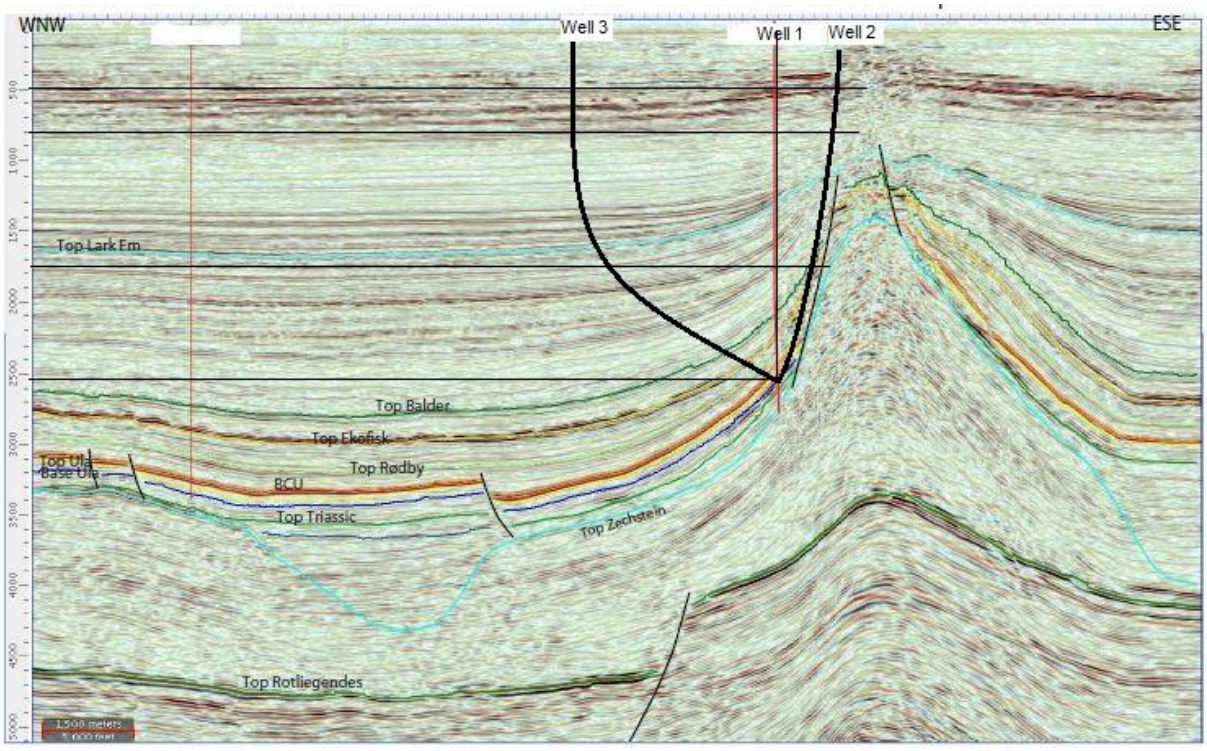

Figure 25: Overview of the examined well trajectories.

Stresses used here are mostly from Geomechanics Technologies, but the maximum horizontal stress has to be estimated as there is no good way of measuring its value. For the purpose of narrowing the possible values for the maximum horizontal value the theory on stress magnitudes at depth and frictional faulting theory, as presented by Moose et al. (1990) and Zoback et al. (2003), will be used (Zoback et al. 2003):

$$\frac{\sigma_1'}{\sigma_3'} = \frac{\sigma_1 - p_p}{\sigma_3 - p_p} = \left[(\mu^2 + 1)^{\frac{1}{2}} + \mu\right]^2 \tag{57}$$

Here σ_1 and σ_3 refers to the largest and smallest stresses, p_p is the pore pressure and μ is the coefficient of friction.

Using equation 57 together with Anderson's faulting theory to decide which of the principal stresses will be largest and smallest. This will give three separate formulas; one for normal faulting, one for strike slip faulting and one for reverse faulting. Figure 26 gives an example of how the end result might look like.

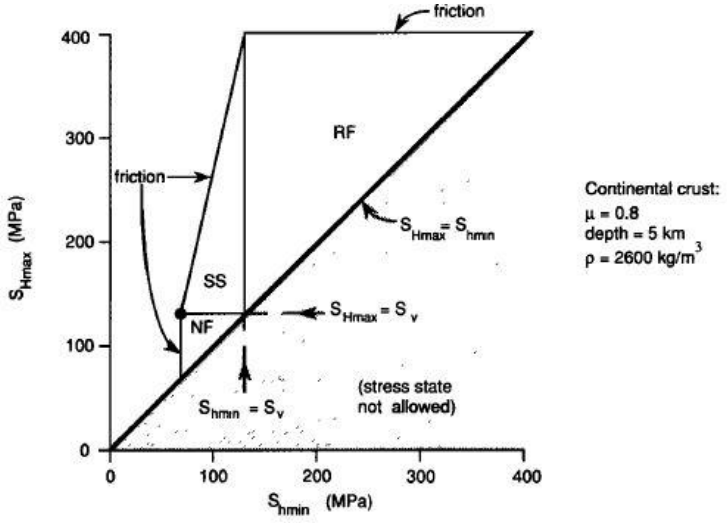

Figure 26: Allowable stresses for the example to the right of the graph (Moos and Zoback 1990).

The steps for constraining the value of the maximum horizontal stress was: Read of a value for the vertical stress and create graph for allowable stresses, read of a value of the minimum horizontal stress and plot this value onto graph for allowable stresses, assume faulting region and note down upper and lower σ_{Hmax} values. This method will only give approximate values, but for depth 2868.7 m the value of σ_{Hmax} was 58,4 MPa whilst the values found using the method described here gave the range 60-73,5 for 2900 m, showing some correlation to the theory used here. For read values of σ_{hmin} that end outside of this range the following expression is used to give an estimate of σ_{Hmax} (Fjær et al. 2008, 159):

$$p_{w,max}^{frac} = 3\sigma_h - \sigma_H - p_p + T_0 \quad (58)$$

$p^{frac}_{w,max}$ is the fracturing pressure.

Equation 58 should be used together with an XLOT test, here it is used with LOT tests performed at same depths around the salt structure to give an idea of what σ_{Hmax} might be. It is assumed that the value gained from equation 58 will give a high value of σ_{Hmax}.

As for the stress directions it will be assumed that up to a certain distance from the salt the maximum principal stress direction will be perpendicular to the salt (Nikolinakou, Flemings, and Hudec 2013). At greater distances a small rotation towards horizontal direction is assumed.

From the pore pressure interpretations given in appendix A, well 8/10-5 S and 8/10-6 S located at Butch SW and Butch East has higher pore pressure gradients than well 8/10-4 S located at Butch Main. The pore pressures from well 8/10-4 S will be preferred in this report, but if the differences are sufficient some modification to it might be done.

For the mud windows shown in the results section, the well temperature has been set to the same temperature as the formation. As the general trend is that a lower wellbore temperature gives better stability, the assumption used here might give too narrow ranges for the mud windows. Also a detailed value of the strength parameters would maybe sway the stable range.

4.4. Results

In this section the results of the calculations done with PSI will be presented. Several different parameters have been checked, and some will be presented here. For each depth the results for the same factors will be presented, so that the impact of the salt and the stress perturbations caused by the salt can be seen.

PSI, Preventing Shale Instabilities, is a program developed by Sintef. With PSI the user can generate mud weight windows and sensitivities for a wide range of parameters, check the borehole cross section, check stability versus time and specify uncertainty. The program is based on a poroelastic model that describes the elastic stresses around a borehole in a linearly elastic formation. Plasticity is added as perturbations to the elastic solution, its implication on borehole stability is discussed in section 4.5. PSI estimates the stability of the hole by testing the stress and pore pressure conditions inside the borehole wall. The mud weight window has weight on the x-axis, and probability of failure one the y-axis. There is a mud window as long as the chance of failure lies below 50 % probability. PSI tests the effective stresses against a set of failure criteria. The tensile failure criterion will give tensile failure when the minor principal stress is tensile, and exceeds the tensile strength, no matter the orientation of the principal stresses. For shear failure the user can choose between Mohr-Coulomb, Drucker-Prager and Modified Lade. There is also a possibility to include weak plain failure criteria. Simplifying assumptions in PSI:

- One of the principal in situ stresses is vertical
- p_w is kept constant after drilling
- The borehole temperature remains constant after drilling.
- The rocks permeability is not affected by the presence of the borehole.
- The stresses around the borehole are not affected by failure elsewhere.

The results in this section is generated using a student version of PSI. For the calculations done here, the physical criteria, shear and tensile failure, will be used. This program assumes the principal stresses are parallel and perpendicular to a vertical wellbore. Where the principal stresses have rotated around the salt, a redefinition of the stress directions has to be done. This simply means that for a vertical well close to the salt, there might have to be put on an inclination in PSI, so as to get correct results. The modified lade criteria was utilized. Input parameters available are given in table 6.

Wellbore Data	Well pressure and temperature, inclination, azimuth relative to maximum horizontal stress, time since drilling, Viscosity mud filtrate, NaCl, KCl and $CaCl_2$ content, borehole diameter, depth of investigation and capillary pressure.
Formation Conditions	Vertical stress, largest horizontal stress, smallest horizontal stress, pore pressure, formation temperature and depth
Formation Properties	UCS, friction angle, tensile strength, Young's modulus, Poisson's ratio, Biot's constant, thermal expansion coefficient, porosity, relative volume of smectite, CEC, chemical activity of shale, permeability, Holt's constant, plastic strain index, Weak plane relative strength, relative friction angle, relative tensile strength, inclination, azimuth and plastic strain index.

Table 6: Overview of the available input parameters into PSI, Preventing Shale Instabilities.

The following table of parameters are pre-entered into PSI, and are used at all depths for the stability calculations. Most have minimal impact on the mud weight window. Parameters with an impact are discussed in section 4.5.

Parameter	Value
Viscosity mud filtrate (cPoise)	1
NaCl, KCl and $CaCl_2$ content (weight %)	3.5, 0, 0
Biot's constant	0.915
Thermal expansion coefficient ($1/^0C$)	$1x10^{-5}$
Relative volume of smectite	0.571
CEC (meq/100g)	65.47
Chemical activity of shale	0.982
Holt's constant	0.330

Table 7: Pre-entered parameters used for calculations in PSI.

Holt's constant is a geometrical factor accounting for the orientational distribution of clay mineral grains, typical value is h=0.33. CEC stands for cation exchange capacity. The chemical activity of the shale is the chemical activity of the pore water in the shale.

4.4.1. 500 m

This depth was chosen because it was assumed not to have been affected by the salt, and therefore could give a picture of a mud window for a normal environment would look like. The formation and wellbore temperature was set to 20.3 ^{0}C, using a gradient of 0.0406 ^{0}C/m.

Parameters	**Value**	
Wellbore diameter (inches)	17.5	
Well temperature (^{0}C)	20.3	
Time since drilling (days)	1	
Depth of investigation (mm)	15.56	
Inclination (Degrees)	Well 1, 2, 3	0
Unconfined strength (MPa)	12.5	
Tensile strength (MPa)	1.25	
Friction angle (Degrees)	18.93	
Young's modulus (GPa)	2.48	
Poisson's ratio	0.375	
Porosity	0.35	
Permeability (Darcy)	$1x10^{-9}$	
Vertical stress (MPa)	Well 1	15
Largest horizontal stress (MPa)	Well 1	11-15
Smallest horizontal stress (MPa)	Well 1	11
Formation temperature (^{0}C)	20.3	
Plastic strain index	0.310	
Pore pressure(MPa)	5.1	

Table 8: Input parameters for wellbore stability simulations in PSI, Preventing Shale Instabilities, at 500 meters.

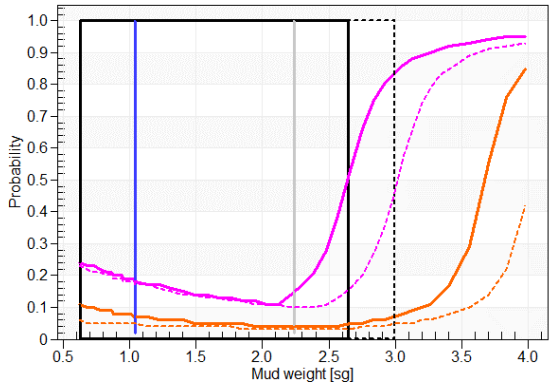

Figure 27: Mud weight window for well 1 at 500 m, generated using PSI. The pink line shows the probability of tensile failure, whilst the orange is for shear failure. The dotted lines are for the lower case of σ_H.

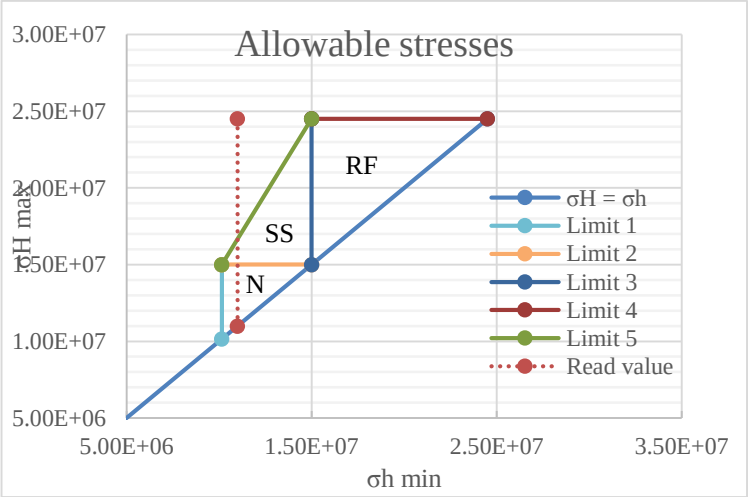

Figure 28: Allowable stresses at 500 m showing all the different faulting regimes; N is normal faulting, SS is Strike slip faulting and RF is reverse faulting.

Since this depth is unaffected by the salt, it is assumed to be within the normal faulting area in figure 28. Two values for σ_{Hmax} can then be read of, and the mud weight window in figure 27 can be generated.

Because of its shallow depth and distance from the salt, there is nothing that sticks out at this area. The possibility of gas that has leaked from the reservoir should be checked.

4.4.2. 800 m

At 800 m it is assumed that the wells 1 and 2, will be in the normal faulting area shown in figure 18. This means that the stresses here are slightly perturbed by the salt, but it is still a normal faulting area. Well 2 is assumed to have a slight inclination of 9 degrees. Results from well 3 is not presented here, as it is similar to well 1. The formation and wellbore temperature was set to 32.48 ^{0}C, using a gradient of 0.0406 ^{0}C/m.

Parameters	**Value**	
Wellbore diameter (inches)	17.5	
Well temperature (^{0}C)	32.48	
Time since drilling (days)	1	
Depth of investigation (mm)	15.56	
Inclination (Degrees)	Well 1, 2, 3	0
Unconfined strength (MPa)	12.5	
Tensile strength (MPa)	1.25	
Friction angle (Degrees)	18.93	
Young's modulus (GPa)	2.48	
Poisson's ratio	0.375	
Porosity	0.3	
Permeability (Darcy)	$1x10^{-9}$	
Vertical stress (MPa)	Well 1	19
	Well 2	30
Largest horizontal stress (MPa)	Well 1	15-19
	Well 2	25
Smallest horizontal stress (MPa)	Well 1	15
	Well 2	15
Formation temperature (^{0}C)	32.48	
Plastic strain index	0.310	
Pore pressure (MPa)	7.93	

Table 9: Input parameters for wellbore stability simulations in PSI, Preventing Shale Instabilities, at 800 meters.

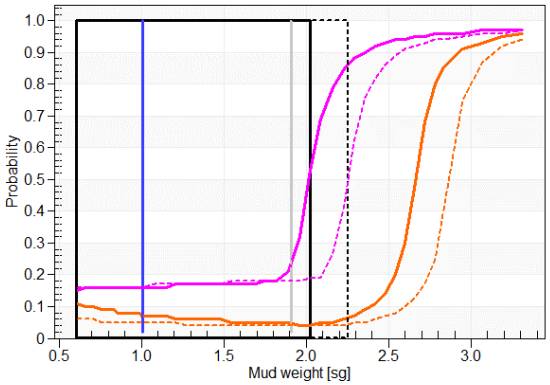

Figure 29: Mud weight window for well 1 at 800 m. With σ_v= 19 MPa, σ_h= 15 MPa, σ_H= 15-19 MPa, giving a good range for both maximum horizontal stresses. The pink line shows the probability of tensile failure, whilst the orange is for shear failure, blue vertical line is pore pressure and grey line is minimum horizontal stress. The dotted lines are for the lower case of σ_H.

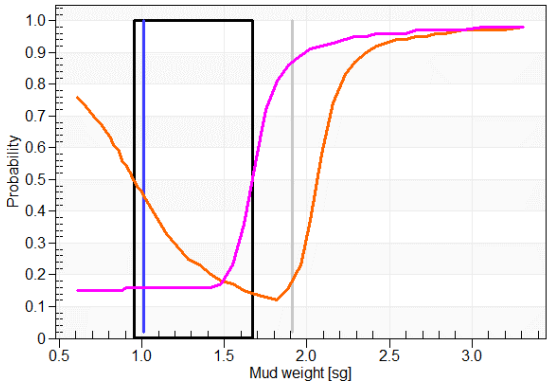

Figure 30: Mud weight window for well 2 with σ_v= 30 MPa, σ_h= 15 MPa, σ_H= 25 MPa. The narrow window is attributed to the high σ_H value, it is assumed that this value is probably lower. The pink line shows the probability of tensile failure, whilst the orange is for shear failure, blue vertical line is pore pressure and grey line is minimum horizontal stress.

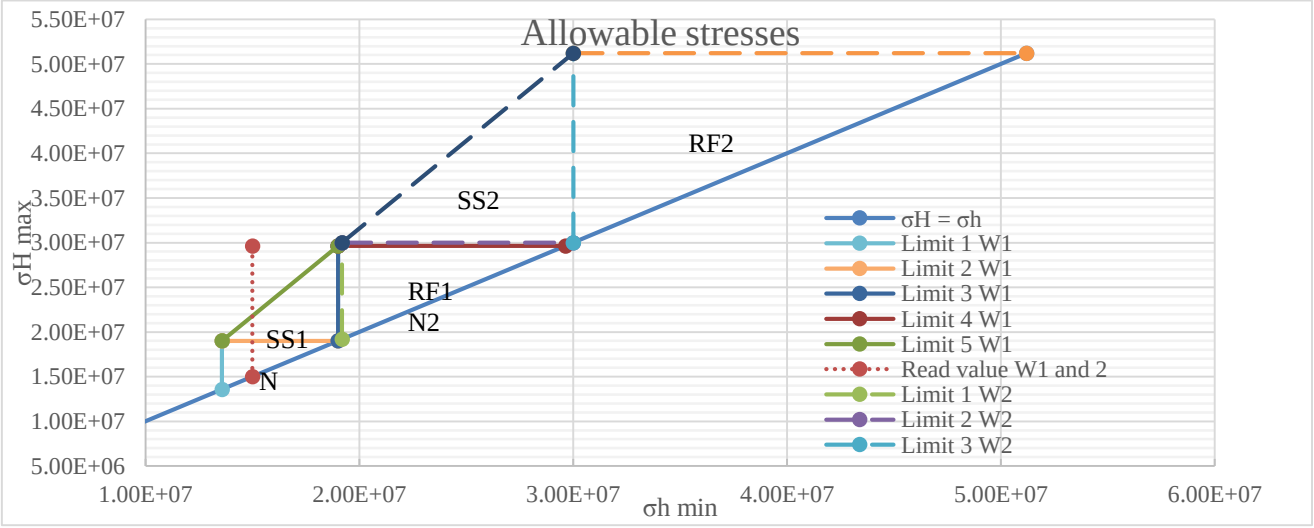

Figure 31: Allowable stresses at 800 m for wells 1, hard lines, and well 2, dotted lines.

As one can see from the two different mud weight windows in figures 29 and 30, finding a good value for σ_{Hmax} is very important. For well 2 the value was set at 25 MPa, because the read value of σ_h was outside the "allowable stresses" in figure 31, whilst the minimum horizontal stress was 15 MPa. The difference between the horizontal stresses therefore increase the chances of shear failure, as is seen on figure 30. The value of σ_H was chosen using an LOT test from a well located to the east of the butch structure, the uncertainty for this value is therefore high and is possibly lower than the one used.

Several factors where checked for their sensitivity, like the azimuth relative to the maximum horizontal stress. For the different values of σ_H this was checked on 0 and 90 degrees to see its

effect on the mud weight window and on the well inclination. For well 1 an azimuth of 0 degrees shows no impact on the well inclination, whilst for an azimuth of 90 degrees a well inclination of 90 degrees can give a 0.8 SG higher upper mud weight, compared to 0 degrees inclination of the wellbore. For well 2 a valid mud weight window is between 0-40 degrees and 0-30 degrees inclination for 0 and 90 degrees azimuth relative to the maximum horizontal stress respectively.

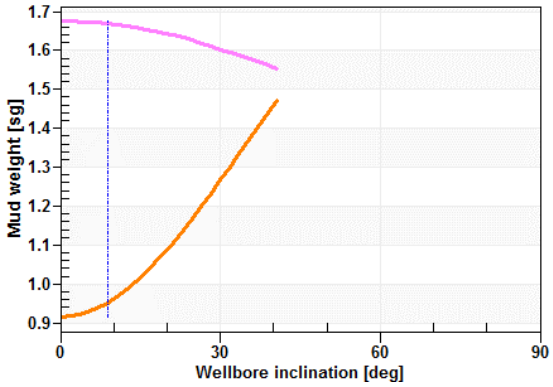

Figure 32: How the mud weight window for well 2 at 800 m will change with wellbore inclination, when azimuth relative to the maximum horizontal stress equals 0 degrees.

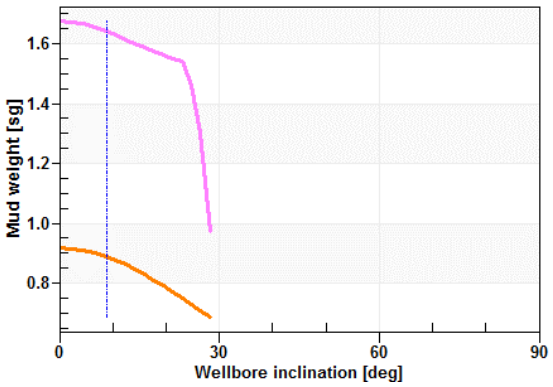

Figure 33: How the mud weight window for well 2 at 800 m will change with wellbore inclination, when azimuth relative to the maximum horizontal stress equals 90 degrees.

A low friction angle and high σ_H makes this trajectory more unstable than for well 1, and the possible wellbore inclinations.

4.4.3. 1750 m

At 1750 m well 1 and 2 will be moderately and strongly affected by the salt. Well 3 is located further away from the salt and is assumed not to be affected. Well 1 is vertical, well 2 and 3 has an approximate inclination of 20 degrees. From the mud windows it is clear that the salt has a strong effect on the stabile range. The pore pressure read of from well 8/10-4S was very low compared to the other two wells given in the appendix, a pore pressure of 1.3 was therefore used for the stability calculations. The formation and wellbore temperature was set to 71.05 ^{0}C, using a gradient of 0.0406 ^{0}C/m.

Parameters	**Value**	
Wellbore diameter (inches)	12 ¼	
Well temperature (^{0}C)	71.05	
Time since drilling (days)	1	
Depth of investigation (mm)	15.56	
Inclination	Well 1	0
	Well 2	0 (20)
	Well 3	20
Unconfined strength (MPa)	12.5	
Tensile strength (MPa)	1.25	
Friction angle (Degrees)	Well 1	21.08
	Well 2	27.55
	Well 3	21.08
Young's modulus (GPa)	3.09	
Poisson's ratio	0.375	
Porosity	0.28	
Permeability (Darcy)	$1x10^{-9}$	
Vertical stress (MPa)	Well 1	48
	Well 2	40
	Well 3	42.5
Largest horizontal stress (MPa)	Well 1	48-49
	Well 2	51.7
	Well 3	37-42.5
Smallest horizontal stress (MPa)	Well 1	35

	Well 2	28
	Well 3	37
Formation temperature (^{0}C)	71.05	
Plastic strain index	0.310	
Pore pressure (MPa)	22.3	

Table 10: Input parameters for wellbore stability simulations in PSI, Preventing Shale Instabilities, at 1750 meters. The inclination in parenthesis is the actual inclination of the well for well 2.

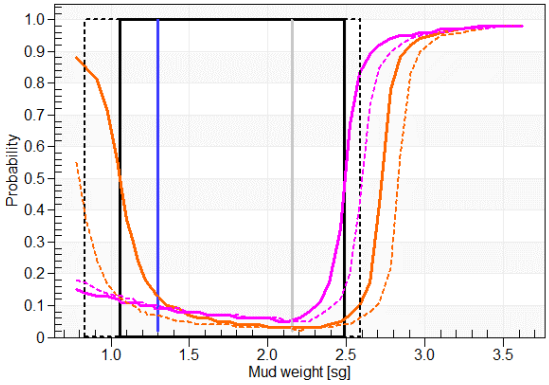

Figure 34: Mud weight window for well 3 at 1750 m. With σv= 42.5 MPa, σh= 37 MPa, σH= 37-42.5 MPa, giving a narrow window. The pink line shows the probability of tensile failure, whilst the orange is for shear failure, blue vertical line is pore pressure and grey line is minimum horizontal stress. The dotted lines are for the lower case of σ_H.

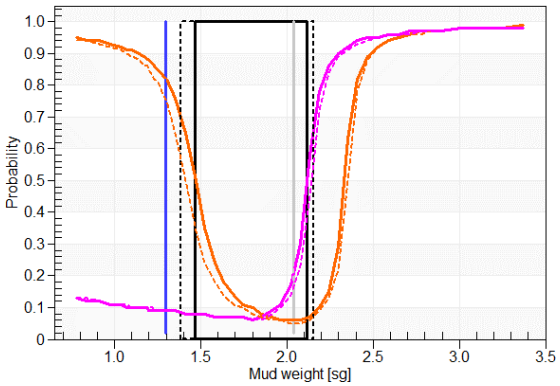

Figure 35: Mud weight window for well 1 at 1750 m. With σ_v= 48 MPa, σ_h= 35 MPa, σ_H= 48-49 MPa, giving a ok range for both maximum horizontal stresses. The pink line shows the probability of tensile failure, whilst the orange is for shear failure, blue vertical line is pore pressure and grey line is minimum horizontal stress. The dotted lines are for the lower case of σ_H.

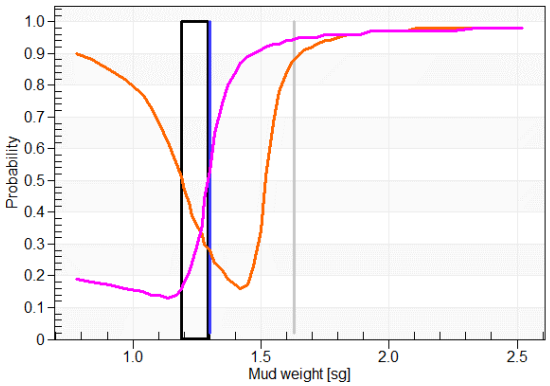

Figure 36: Mud weight window for well 2 at 1750 m. With σv= 40 MPa, σh= 28 MPa, σH= 51.7 MPa, giving a narrow window. The pink line shows the probability of tensile failure, whilst the orange is for shear failure, blue vertical line is pore pressure and grey line is minimum horizontal stress. The dotted lines are for the lower case of σ_H.

Well 3 shows no perturbation from the salt dome at this depth and has a wide mud weight window. For well 2 the effect of the salt is evident when compared to well 3. Higher vertical and maximum horizontal stresses and lower minimum horizontal stresses in wells 1 and 2 gives higher shear forces and narrow mud weight windows, this is especially evident in well 2. In well 2 the same calculations for the maximum horizontal stress, radial stress, as at 800

meters had to be done. Therefore the maximum horizontal stress is most likely higher than the actual value, which has a strong effect on the stability this close to the salt. Also because of the dipping beds adjacent to the salt, well 2 will hit Balder formation at 1750 meters, giving it a higher friction angle. A lower friction angle than 27.55 will not give any possible mud weights. Figure 25 shows some of the formation around Butch.

Because the radial stress emitting from the salt is assumed to be a maximum principal stress, the vertical direction was redefined to follow the wellbore, so that PSI would give the correct results. This means an inclination of 0 degrees was used in the stability calculations within PSI.

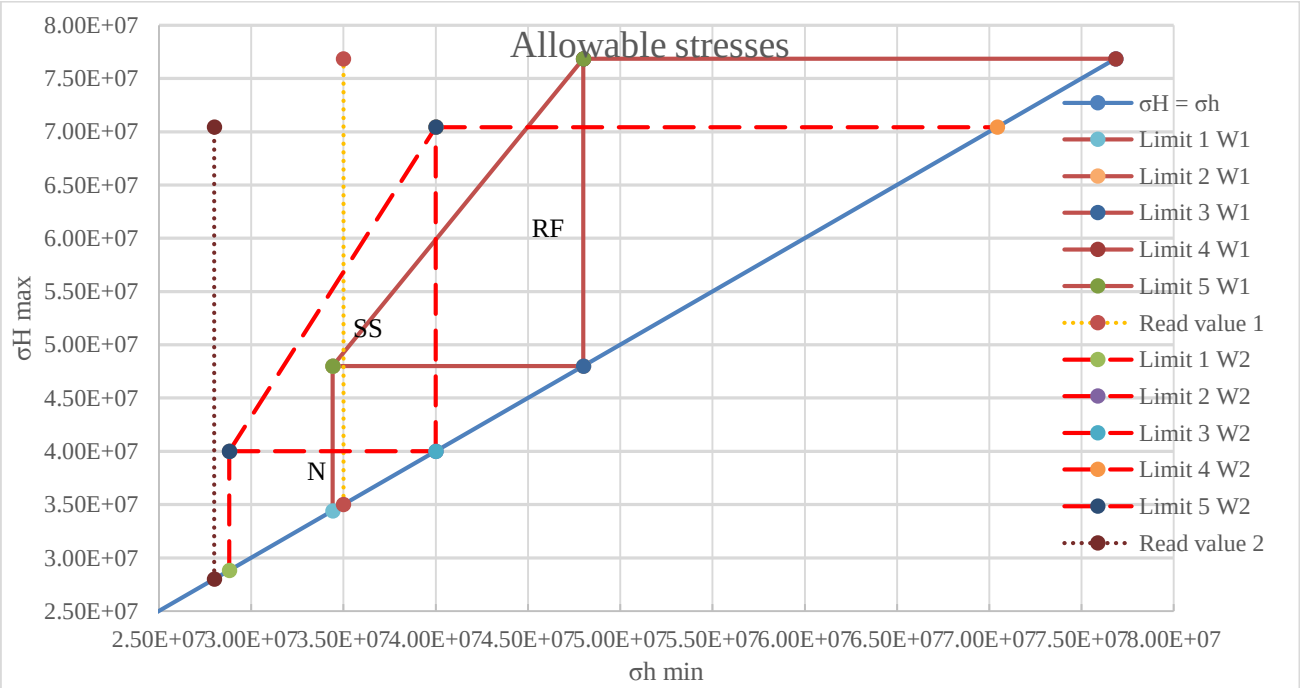

Figure 37: Allowable stresses at 1750 m for wells 1, hard lines, and well 2, dotted lines.

As for 800 m the effect of the azimuth relative to the maximum horizontal stress was investigated. Figures 38 and 39 shows the effect on wellbore inclination of this parameter for 0 and 90 degrees respectively. For well 1 the wellbore inclination has no effect on the mud weight window when the azimuth is 0 degrees, at 90 degrees the mud weight goes from 2.1 SG at 0 degrees wellbore inclination to 3.3 SG at 90 degrees inclination.

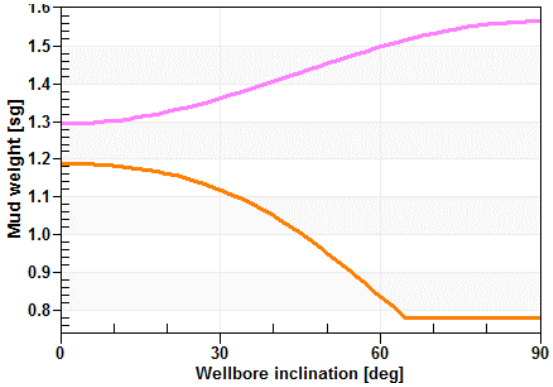

Figure 38: How the mud weight window for well 2 at 1750 m will change with wellbore inclination, when azimuth relative to the maximum horizontal stress equals 0 degrees.

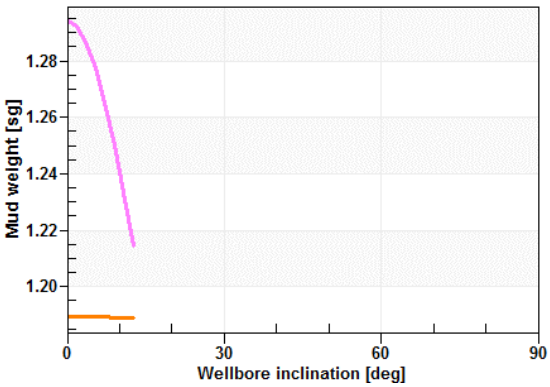

Figure 39: How the mud weight window for well 2 at 1750 m will change with wellbore inclination, when azimuth relative to the maximum horizontal stress equals 90 degrees.

PSI has the ability to include weak planes, which can be thought of as dipping beds. The effect of the dipping beds was investigated for both well 2 and 3, and showed minimum to no impact on the stability of the well. The relative strength and other material values, when changed to half the original, had some effect for certain orientations of the wellbore, but not for the chosen inclinations in well 2 and 3.

4.4.4. 2900 m

Wells 1, 2 and 3 end up at the same point, therefore the stress magnitudes are also assumed to be the same. This depth is assumed to be in the strike slip faulting regime, as described in figure 18. The difference between the three wells are the angels upon which they hit the target. Well 1, 2 and 3 has inclinations of 0, 30 and 50. This does not have a big effect the mud weight windows. The formation and wellbore temperature was set to 117.74 ^{0}C, using a gradient of 0.0406 ^{0}C/m.

Parameters	**Value**	
Wellbore diameter (inches)	8 ½	
Well temperature (^{0}C)	117.74	
Time since drilling (days)	1	
Depth of investigation (mm)	15.56	
Inclination (Degrees)	Well 1	30 (0)
	Well 2	0 (30)
	Well 3	50 (80)
Unconfined strength (MPa)	20	
Tensile strength (MPa)	2	
Friction angle (MPa)	35.87	
Young's modulus (GPa)	14.8	
Poisson's ratio	0.3	
Porosity	0.15	
Permeability (Darcy)	1	
Vertical stress (MPa)	Well 1, 2, 3	60
Largest horizontal stress (MPa)	Well 1, 2, 3	60-73.5
Smallest horizontal stress (MPa)	Well 1, 2, 3	49
Formation temperature (^{0}C)	117.74	
Plastic strain index	0.310	
Pore pressure (MPa)	40.4	

Table 11: Input parameters for wellbore stability simulations in PSI, Preventing Shale Instabilities, at 1750 meters. The inclination in parenthesis is the actual inclination of the well.

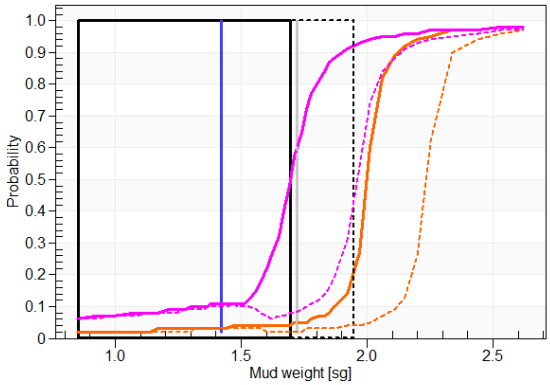

Figure 40: Mud weight window for well 1 at 2900 m. With σv= 60 MPa, σh= 49 MPa, σH= 60-73.5 MPa, giving a narrow window. The pink line shows the probability of tensile failure, whilst the orange is for shear failure, blue vertical line is pore pressure and grey line. The dotted lines are for the lower case of σ_H.

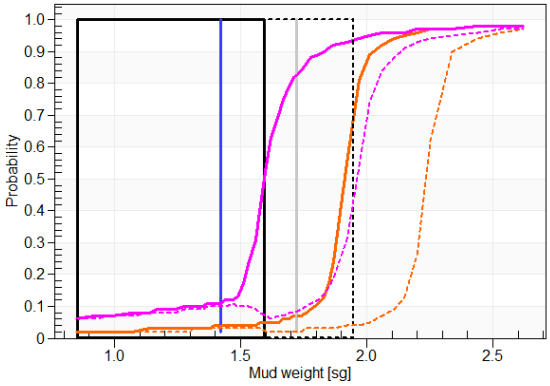

Figure 41: Mud weight window for well 2 at 2900 m. With σv= 60 MPa, σh= 49 MPa, σH= 60-73.5 MPa, giving a narrow window. The pink line shows the probability of tensile failure, whilst the orange is for shear failure, blue vertical line is pore pressure and grey line. The dotted lines are for the lower case of σ_H.

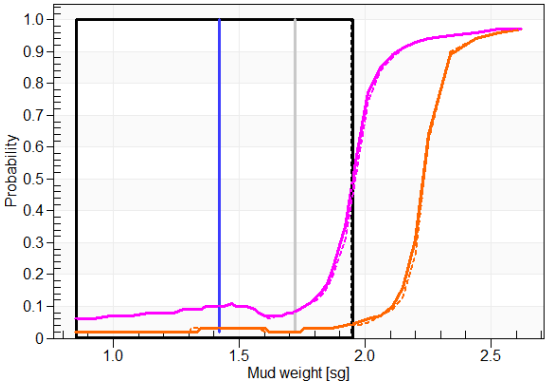

Figure 42: Mud weight window for well 2 at 2900 m. With σv= 60 MPa, σh= 49 MPa, σH= 60-73.5 MPa, giving a narrow window. The pink line shows the probability of tensile failure, whilst the orange is for shear failure, blue vertical line is pore pressure and grey line. The dotted lines are for the lower case of σ_H.

Figures 40-42 shows that the different inclinations does not affect the mud window much, but as at 1750 m, well 2 has smaller mud window for the higher value of σ_{Hmax}. The high inclination on well 3 shows that even an increase on 13.5 MPa on the maximum horizontal stress does not have a noticeable effect on the stability of this well at this depth.

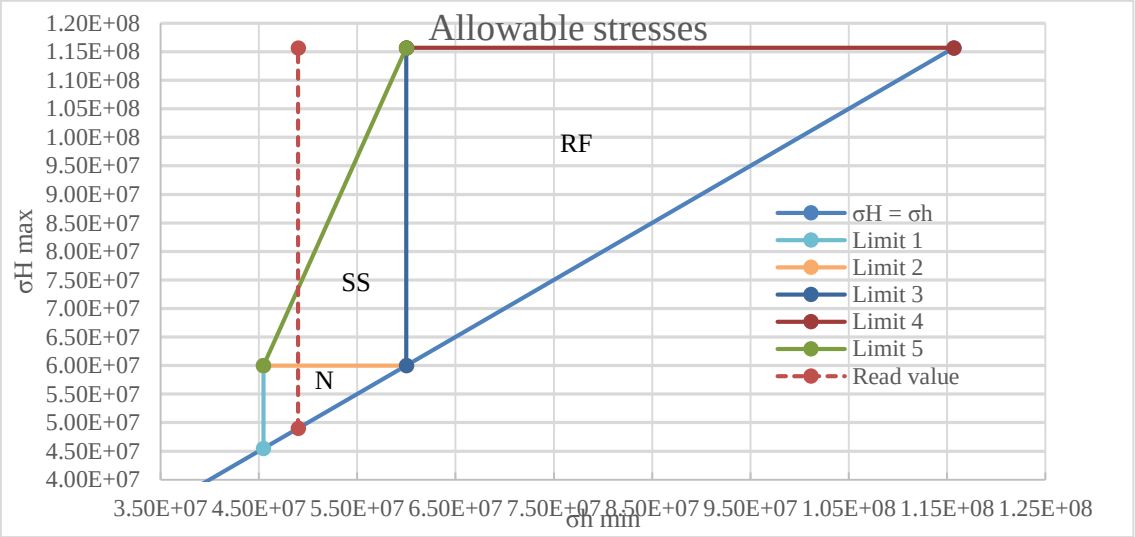

Figure 43: Allowable stresses at 2900 meters.

The azimuth relative to the maximum horizontal stress did have some effect on how the wellbore inclination would affect the mud weights, at 0 degrees azimuth there was barely any effect. For an azimuth of 90 degrees figure 44 gives the variation of mud weights over inclinations 0-90 degrees for well 1, the trend is similar for the other two wells.

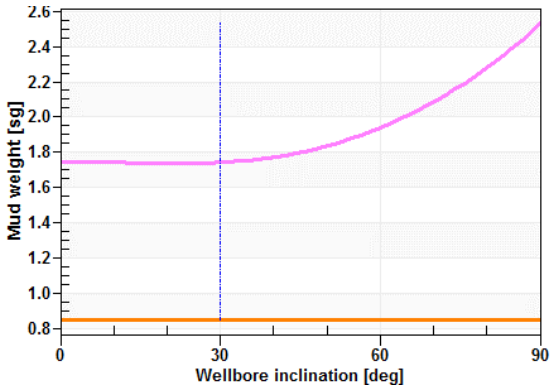

Figure 44: How the mud weight window for wells 1 with σ_{Hmax}=73.5 at 2900 m will change with wellbore inclination, when azimuth relative to the maximum horizontal stress equals 90 degrees.

Because of the high inclination of well 3, the mud weight window will vary with the azimuth direction. For σ_{Hmax}= 60 MPa the best directions is at 90 and 270 degrees, for σ_{Hmax}= 73.5 there are four tops at 50,110, 230 and 280 degrees.

As for the other depths the well temperature has when doing the calculations has been set equal to the formation temperature. A greater mud window would be obtained by lowering the wellbore temperature.

4.5. Discussion

There are some formal rules related to wellbore stability. The mud weight should be kept above the pore pressure in order to prevent influx of fluids from the formation. The upper limit is set at the minimum horizontal stress. This is to prevent fracking the formation and in the process loose mud into the formation. Going outside these limits can lead to kicks and blowouts. In this text, when the term mud weight window is used, the two mentioned limits are the range of mud weights that can be used if nothing else is mentioned.
Salt which intrudes into the formations above it might have an impact on the stresses for ranges several times its own radius. Section 4.4 presents the results of the stability calculations done for three different wells around the butch salt dome. This section discusses the results gathered.

In any wellbore stability analysis, the most important factors are the stresses. Their direction and value at the wellbore will have major implications for whether or not the well will be stable. All three principal stresses will, if investigated, show a great sensitivity on the mud weight window. In a complex stress environment, as the one seen around salt structures, misreading the values by only a few MPa can be the difference between success and failure for the well. The general trend in a normal faulting area, by changing one value and keeping the others fixed, is that an increase in σ_{Hmax} narrows the range of mud weights, increasing σ_{hmin} widens the range of mud weights and σ_v has a more concave shape with the highest range of mud weights somewhere in the middle. From the calculations done, tensile failure is sensitive for all changes in stress values at all depths, whilst shear stresses start to respond only at greater depths. This is because of the relative values of the horizontal stresses, as it is seen in the difference between well 1 and 2 at 800 meters. For well 1 the shear failure is largely unresponsive to any meaningful changes in stress values, but for well 2 where the σ_{Hmax} is much greater, shear failure is responsive. Close to the salt, especially in the upper parts, the stress magnitudes are more likely to be at the extremes, where any change to one of them will restrict the stability to the point of failure. The response of the shear failure was further checked up against the friction angle of the formation. By having a higher friction angle, the shear failure required higher values of the horizontal stresses in order to be affected. For a high stress environment, a reasonably high friction angle is required in order to avoid shear failure. If, for example, well 2 at 1750 had a lower friction angle than 27.55, there

would be no mud weight window at all, even with the current friction angle the well would most likely fail at this depth.

σ_{Hmax} is hard to correctly find the magnitude for. As explained in section 4.3, using frictional faulting theory together with Andersons faulting theory can help constrain the magnitudes of this principal stress. From figure 13 one can see that the minimum horizontal stress adjacent to the salt is lower than for the far field values. This, together with zones of lowered vertical stress can make the read value of σ_{hmin} fall outside the range using equation 57 and Andersons faulting theory. In order to restrict σ_{Hmax}, Dussealt et al. (2004a) used the same expression as the one given in equation 57 together with LOT data, where it was assumed that $p_F = \sigma_{hmin}$. The three different methods where compared, and the results show a satisfying correlation with each other. It should be noted that some of the LOT data are from wells on on the eastern and southwestern side of Butch. As pointed out in section 4.4, the values calculated using equation 58 and LOT data seems to give a too high value of σ_{Hmax}.

Depth	**Calculated σ_{Hmax} using equation 57 and Andersons faulting theory (MPa).**	**Calculated σ_{Hmax} using equation 58 and LOT (MPa). (2900 was calculated in Weatherford report.)**	Calculated σ_{Hmax} using equation 57 and LOT (MPa).
500 (LOT at 428)	11-15		14.8
800 (LOT at 719)	15-19 (well 1 and 3)	25 (well 2)	17.6
1750 (LOT at 1760)	48-49 (well 1) 37-42.5 (well 3)	51.7 (well 2)	43.5 and 49.5
2900 (LOT at 2869)	60-73.5 (well 1, 2, 3)	58.4	66.9

Table 12: Column 2 is showing the range of values for each well, marked when necessary. Column 3 shows the calculated values using equation 44 and fracture pressures from LOT data around Butch. Column 4 shows the calculations done using equation 3 and LOT data from around Butch. The values marked with well 1,2 or 3, are the ones used for the stability analysis in those wells.

The most favorable direction to drill in an isotropic elastic rock is in parallel to the maximum principal stress, and least stable parallel to the intermediate principal stress (Fjær et al. 2008, 319). In the case of a salt structure like Butch, the maximum and intermediate principle stress will change with proximity to the salt wall. Close to the salt wall the radial force perpendicular from the salt is the maximum principal stress, whilst the overburden stress is

the intermediate. Further away, these two change. Examining the azimuthal influence on the sensitivity of the wellbore inclination can indicate this behavior. For wells 1 and 3 drilling with an azimuth of 90 degrees relative to the maximum horizontal stress, or intermediate principle stress, will give a higher mud weight window as inclination increases. Meaning that drilling horizontally towards the minimum principal stress is most stable, as the tensile failure limit increases. For well 2 the results are quite different. At 800 meters the best direction would be to drill vertically with an azimuth of 0^0 relative to the maximum horizontal stress, as seen in figure 32. Drilling at 90^0 azimuth at this depth would, as seen in figure 33, be less stable. Well 2 at 1750 has the greatest mud weight window for a well directly towards the salt, in the direction of the greatest principal stress, seen in figure 38. Drilling perpendicular to the maximum principal stress severely restricts the wellbore inclinations allowed, figure 39.
The difference between these wells and the wellbore inclination response to azimuthal direction is the size of σ_{Hmax}. Although well 1, at 1750 meters, is in the strike slip region, the influence from the salt on the maximum horizontal stress is not great enough to severely affect the stability in any direction. Meaning that at this distance at any depth, the salt will not have perturbed the stresses too much compared to a normal faulting regime.
At 2900 meters the azimuthal directions influence on the mud weight window is similar to the described behavior for wells 1 and 3 at shallower depths. This is attributed to the analysis depth, and the fact that the salt dome has not "pushed" so much into the formation here and the stress re-orientation is not as great because of the low angle slope of the salt at this depth.
The investigation into the azimuthal direction compared to proximity of the wellbore and the salt, shows that close to the salt the best direction to drill is towards to the salt wall. Also the most unstable region is closer to the top of the salt dome, as this area has high values of σ_{Hmax} and low values of σ_{hmin}, leading to increased shear forces. As seen from well 2 at 1750 it is dangerous to drill close to the salt at this area. This is more or less in line with the predicted stability issues Dussealt et al. (2004a), and is also seen in figure 18.

Holt et al. (2015) investigated the brittleness of shales, and their relevance to borehole collapse and hydraulic fracturing. They found that brittleness is a key factor in triggering borehole collapse, as drilling experience over the last decade indicates that plastic deformation enhances borehole stability (Fjær et al. 2008). Rock mechanics has a number of measurements that could quantify brittleness. The factor B_1 is one of these measurements. It is defined as the elastic part of the total strain prior to rock failure (Holt et al. 2015). B_1 is found by using triaxial tests, although the value will vary with test procedure and equipment.

Incorporating some form of a plasticity measurement into borehole stability models can make the difference between a stable and unstable hole. In the program, PSI, used for stability simulations here, the plastic strain index is an attempt to take into account the brittleness and its effect on wellbore stability. The plastic strain index is by definition equal to $1 - B_1$ (Holt et al. 2015). Holt et al. (2015) found that brittleness decreases with increasing confining pressure. High porosity, low strength overburden shales were found to behave more plastic than stronger, lower porosity gas shales, as the decay of brittleness with confinement was more rapid for the overburden shales. In general, brittleness decreases with increasing confining pressure. Holt et al (2015) found that at lower stresses the brittle-ductile transition is characterized by dilatancy prior to failure and a loss of load bearing capacity after failure. For higher stresses a bigger part of the deformation prior to failure is plastic, and strain hardening may occur after failure. They also found that brittleness is higher for loading parallel to bedding than perpendicular to it, meaning a wellbore is less plastic parallel to bedding planes and hence less stable. A possible way to increase plasticity could be to expose the shale to KCl brine. Figure 45 clearly shows the major impact of plasticity on borehole stability for well 2 at 1750 meters. The plastic strain index is a critical component of stability in shales, yet it is not understood well enough.

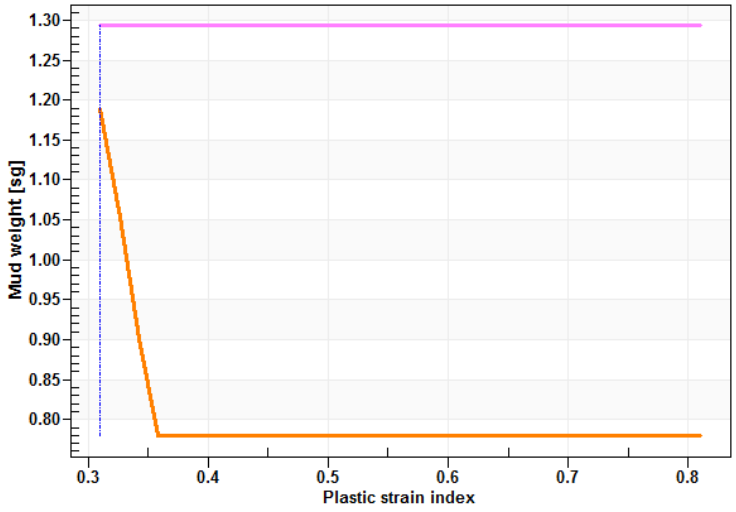

Figure 45: Sensitivity of the plastic strain index for well 2 at 1750 meters. There is clearly a strong effect on wellbore stability.

Temperature is one way of mitigating the possibilities of wellbore failure. For the results in section 4.4, a wellbore temperature equal to the formation temperature was used. Simply by reducing the temperature in the wellbore, a wider mud weight window can be achieved, especially in areas where the shear forces are high. This is relevant to the stability of wells that is wished to be close to the salt. It is worth noting that changes in formation properties,

such as UCS, tensile strength and friction angle will change the range of temperatures for achieving a stable wellbore. Figure 46 is an example of the wellbore temperatures effect on the stability.

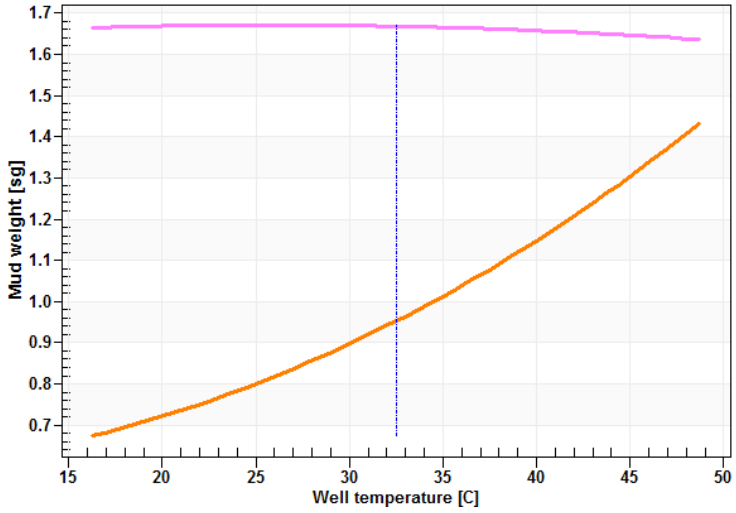

Figure 46: The sensitivity of wellbore temperature on the mud weight window for well 2 at 800 meters.

The importance of finding material properties that are accurate is a major part of any stability exercise. A greater unconfined strength and friction angle will lower the risk of shear failure in zones of high shear stresses, giving a larger mud window. Permeability has a large impact on the mud weight window. Higher permeability in well 2 at 1750 meters would greatly improve the mud weight window. The end effect of choosing material properties as close to the reality as possible is choosing the right trajectory, especially in medium to high shear stress areas as around salt domes. As an example the unconfined strength is shown in figure 47 and 48 for well 1 and 3 at 1750 meters. Closer proximity to the salt wall will make the importance of good material properties values greater, as can be seen from the increased sensitivity from well 3 to well 1.

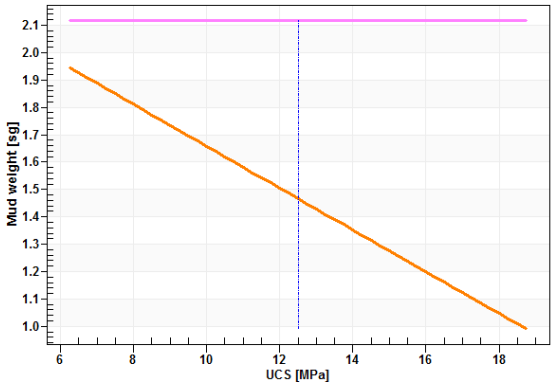

Figure 47: Unconfined strength and its effect on the mud weight window for well 1 at 1750 m.

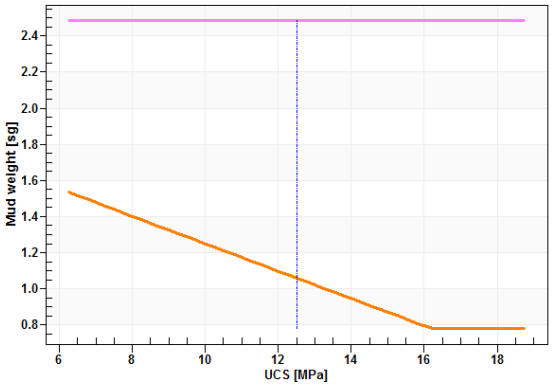

Figure 48: Unconfined strength and its effect on the mud weight window for well 3 at 1750 m.

The effect of the bedding planes was also examined, as it may have a decisive impact on the stability of inclined wells (Fjær et al. 2014). In the literature it is called planes of weakness, and there are several models which fits different rocks. Fjær et al. (2014) tested three different shales in their paper, and concluded that all three types showed significant strength anisotropy. This does not conclude that every rock has this trait.
For the stability calculations in this thesis, the bedding plane does not seem to have an effect. Even when the relative UCS, tension strength and friction angle was reduced by 50 % there was no effect on the stability of the wellbore for any depth in any of the wells.

5. Guidelines

A. The geometry of the salt body is important, as different geometries affects its surroundings differently. A long, relatively flat, salt sheet will have reduced horizontal stresses above and below, whilst the vertical will remain unchanged or increase a little. A connected diapir, like Butch, will have increased radial stresses adjacent to the salt, reduced hoop stress because of circumferential expansion and areas of lower vertical stress, especially towards the top of the salt.

   A salt wall will have reduced minimum principal stresses at the ends, whilst at the sides the minimum principal stress can interchange between increased and decreased values (Koupriantchik et al. 2005).

   Convex curves shows a decrease in the minimum principal stress, and an increase in the von Mises stress. This gives a smaller mud weight window

   Concave curves shows an increase in the minimum principal stress, and a decrease in the von Mises stress. This gives a better mud weight window.

B. Find the composition, density and relative distribution different salts in the salt structure. It will have an impact on the distribution of stresses. Connected salt with density lower than the surrounding sediments will cause a reduction of the vertical stresses adjacent to the salt, if the density is higher the opposite will take place (Sanz and Dasari 2010).

C. The most unstable region is closer to the top of the salt dome, as this area has high values of σ_{Hmax} and low values of σ_{hmin}, leading to increased shear forces.

   It is therefore recommended to stay clear of the top section of salt domes. An approximate distance of 0.5 x diameter of the top of salt is recommended as a rule of thumb. If the drilling goes any closer, it is recommended to drill towards the salt. At deeper sections with a shallow slope, the formation is more stable and the restrictions for the upper part does not apply. The stress perturbations in the deeper sections may be small enough to allow to drill with azimuth of up to 90^0.

D. In general it is not advised to drill parallel to the borehole wall, as both strength anisotropy from weak planes and a lower plasticity parallel to bedding planes, might result in unfavorable borehole stability. Also according to Fjær et al. (2008) drilling perpendicular to the largest principal stress, and parallel to the intermediate principal stress is least favorable.

E. Proper stress estimations is the most important aspect regarding wellbore stability. This is especially important the closer one gets to the salt diapir, and or sheet. When reaching the depth at which the salt structure is thought to have affected the stresses, LOT tests should be done so as to have means of estimating the maximum and minimum horizontal stresses.
F. The perturbations from a salt structure will be unique for each geometry and formation setting. It is therefore strongly recommended that a 3D geomechanical model is built. This will give the engineers a way to quickly spot risky zones that should be avoided.
G. Material properties for the formations affected by the salt structure should be given extra attention. Wrong estimates might give a wrong view of the stresses and failure limits for the formations adjacent to the salt.
H. Closer to a salt dome wall, the hoop stress will decrease because of the circumferential expansion of the salt dome, and the maximum principal stress, which is not the radial stress emitting from the salt, will increase. Together this gives an increase in shear forces. It is therefore recommended to decrease the well temperature in order to reduce the risk of shear and tensile failure. The well temperature should decrease with proximity to the salt.

Bibliography

Adachi, Jose, Zsolt Robert Nagy, Colin Michael Sayers, Martiris Smith, and David Francis Becker. 2012. "Drilling Adjacent to Salt Bodies: Definition of Mud Weight Window and Pore Pressure Using Numerical Models and Fast Well Planning Tool." 2012/1/1/.

Al-Ajmi, Adel M, and Robert W Zimmerman. 2006. "Stability analysis of vertical boreholes using the Mogi–Coulomb failure criterion." *International Journal of Rock Mechanics and Mining Sciences* 43 (8):1200-1211.

Belhouchet, Mohamed, and Amdad Ali. 2013. BUTCH FIELD BASIN MODELING AND WELLBORE STABILITY ANALYSIS.

centrica, energi, Petroleum Faroe, Energy Suncor, and Energy Spring. 2012. Operations Geology Final Well Report, Well 8/10-4 S - Butch.

centrica, energi, Petroleum Faroe, Energy Suncor, and Oil Tullow. 2014a. "Operations Geology Final Well Report, Well 8/10-5 S - Butch East ".

centrica, energi, Petroleum Faroe, Energy Suncor, and Oil Tullow. 2014b. "Operations Geology Final Well Report, Well 8/10-6 S - Butch East."

Colmenares, L. B., and M. D. Zoback. 2002. "A statistical evaluation of intact rock failure criteria constrained by polyaxial test data for five different rocks." *International Journal of Rock Mechanics and Mining Sciences* 39 (6):695-729. doi: http://dx.doi.org/10.1016/S1365-1609(02)00048-5.

Costa, A. M., E. Poiate, Jr., C. S. Amaral, C. J. C. Goncalves, J. L. Falcao, and A. Pereira. 2010. "Geomechanics Applied to the Well Design Through Salt Layers In Brazil:A History of Success." 2010/1/1/.

Davison, I, I Alsop, P Birch, C Elders, N Evans, H Nicholson, P Rorison, D Wade, J Woodward, and M Young. 2000. "Geometry and late-stage structural evolution of Central Graben salt diapirs, North Sea." *Marine and Petroleum Geology* 17 (4):499-522.

Dusseault, Maurice B., Vincent Maury, Francesco Sanfilippo, and Frederic J. Santarelli. 2004a. "Drilling Around Salt: Risks, Stresses, And Uncertainties." 2004/1/1/.

Dusseault, Maurice B., Vincent Maury, Francesco Sanfilippo, and Frederic J. Santarelli. 2004b. "Drilling Through Salt: Constitutive Behavior And Drilling Strategies." 2004/1/1/.

Ewy, R. T. 1999. "Wellbore-Stability Predictions by Use of a Modified Lade Criterion." doi: 10.2118/56862-PA.

Fjær, Erling, Rune Martin Holt, Per Horsrud, Arne Marius Raaen, and Rasmus Risnes. 2008. *PETROLEUM RELATED ROCK MECHANICS*. 2 ed: Elsevier B.V.

Fjær, Erling, Jørn F. Stenebråten, Rune M. Holt, Andreas Bauer, Per Horsrud, and Olav-Magnar Nes. 2014. "Modeling Strength Anisotropy." 2014/11/24/.
Fossen, Haakon. 2010. *Structural geology*: Cambridge University Press.
Fredrich, J. T., D. Coblentz, A. F. Fossum, and B. J. Thorne. 2003. "Stress Perturbations Adjacent to Salt Bodies in the Deepwater Gulf of Mexico." 2003/1/1/.
Fredrich, Joanne T., Bruce P. Engler, Jeffrey A. Smith, Ernest C. Onyia, and Davis Tolman. 2007. "Pre-Drill Estimation of Sub-Salt Fracture Gradient: Analysis of the Spa Prospect to Validate Non-Linear Finite Element Stress Analyses." 2007/1/1/.
GeologicalSociety. 2013. Origin and Evolution of Allochthonous Salt Sheets.
Geomechanics Technologies, Geomechanics

Subsurface, AS. 2013. 3D Geomechanical Model and Wellbore Stability Analysis for Butch Field, North Sea. Centrica Energi.
Håpnes, Mats. 2014. "Drilling in Salt Forations and Rate of Penetration Modelling."Master, Department of Petroleum Engineering and Applied Geophysics, Norwegian University if Science and Technology.
Holt, Rune M., Erling Fjær, Jørn F. Stenebråten, and Olav-Magnar Nes. 2015. "Brittleness of shales: Relevance to borehole collapse and hydraulic fracturing." *Journal of Petroleum Science and Engineering* 131 (0):200-209. doi: http://dx.doi.org/10.1016/j.petrol.2015.04.006.
Koupriantchik, Dmitri, Suzanne P Hunt, PJ Boult, and AG Meyers. 2005. "Geomechanical modeling of salt diapirs: 3D salt structure from the Officer Basin, South Australia." Proceedings to the 11th International Conference on Computer Methods and Advances in Geomechanics.
Luo, Gang, Maria-Katerina Nikolinakou, Peter B. Flemings, and Michael R. Hudec. 2012. "Near-salt Stress And Wellbore Stability: A Finite-element Study And Its Application." 2012/1/1/.
Moos, Daniel, and Mark D. Zoback. 1990. "Utilization of observations of well bore failure to constrain the orientation and magnitude of crustal stresses: Application to continental, Deep Sea Drilling Project, and Ocean Drilling Program boreholes." *Journal of Geophysical Research: Solid Earth* 95 (B6):9305-9325. doi: 10.1029/JB095iB06p09305.
Nagy, Z. R., D. W. Lee, C. M. Sayers, T. R. Zapata, and J. L. Silvestro. 2013. "Iterative 3D Geomechanical Modeling to Determine Distribution and Impact of Stresses in Deepwater Gulf of Mexico Subsalt and Near-Salt Environments." 2013/1/1/.
Nikolinakou, M. A., G. Luo, M. R. Hudec, and P. B. Flemings. 2011. "Geomechanical Modeling of Stresses And Pore Pressures In Mudstones Adjacent to Salt Bodies." 2011/1/1/.

Nikolinakou, M. A., M. P. Merrell, G. Luo, P. B. Flemings, and M. R. Hudec. 2013. "Geomechanical Modeling of the Mad Dog Salt, Gulf of Mexico." 2013/1/1/.

Nikolinakou, Maria A., Peter B. Flemings, and Michael R. Hudec. 2013. "Modeling stress evolution around a rising salt diapir." *Marine and Petroleum Geology* 51 (0):230-238. doi: http://dx.doi.org/10.1016/j.marpetgeo.2013.11.021.

Omojuwa, Emmanuel O., Sameul O. Osisanya, and Ramadan Ahmed. 2011. "Properties of Salt Formations Essential for Modeling Instabilities While Drilling." 2011/1/1/.

Sanz, P. F., and G. R. Dasari. 2010. "Controls On In-situ Stresses Around Salt Bodies." 2010/1/1/.

Valencia, Karen, Paulino Villacastin, Linn Tove Brandås, Claudia Amorocho, and Johan Tronvoll. 2012. BUTCH FIELD GEOMECHANICAL MODEL AND WELLBORE STABILITY STUDY. Weatherford Petroleum Consultants AS: For Centrica Energi.

Van Der Zee, Wouter, Jack Taylor, and Martin Brudy. 2012. "Improving Sub Salt Wellbore Stability Predictions Using 3D Geomechanical Simulations." 2012/1/1/.

Zhong, Liguo, Haiyang Cong, Shiqing Wang, Defu Zhao, Zhifeng Wang, and Guang Yang. 2008. "Deep Salt Formation Wells Successfully Drilled with Integrated Techniques in Tahe Oilfield." 2008/1/1/.

Zimmerman, Robert Wayne, and Adel M. Al-Ajmi. 2006. "Stability Analysis of Deviated Boreholes using the Mogi-Coulomb Failure Criterion, with Applications to some North Sea and Indonesian Reservoirs." 2006/1/1/.

Zoback, M. D., C. A. Barton, M. Brudy, D. A. Castillo, T. Finkbeiner, B. R. Grollimund, D. B. Moos, P. Peska, C. D. Ward, and D. J. Wiprut. 2003. "Determination of stress orientation and magnitude in deep wells." *International Journal of Rock Mechanics and Mining Sciences* 40 (7–8):1049-1076. doi: http://dx.doi.org/10.1016/j.ijrmms.2003.07.001.

Appendix A: Usefull formulas

A1 Transformation formulas for the general elastic solution

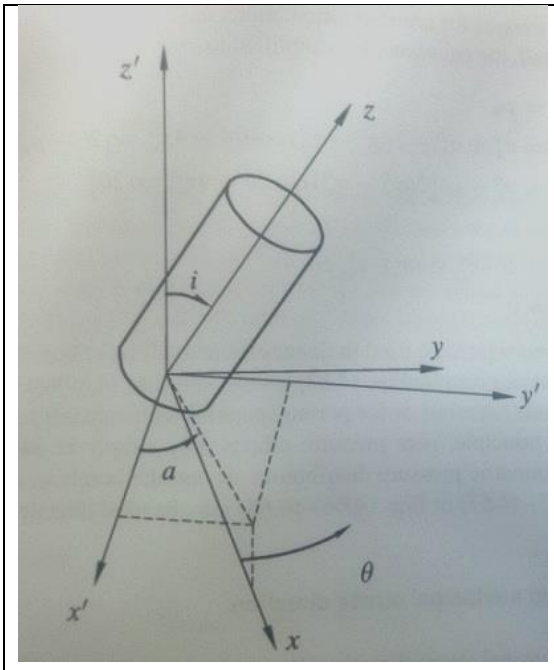

Figure i: Transformation geometry (Fjær et al. 2008, 147).

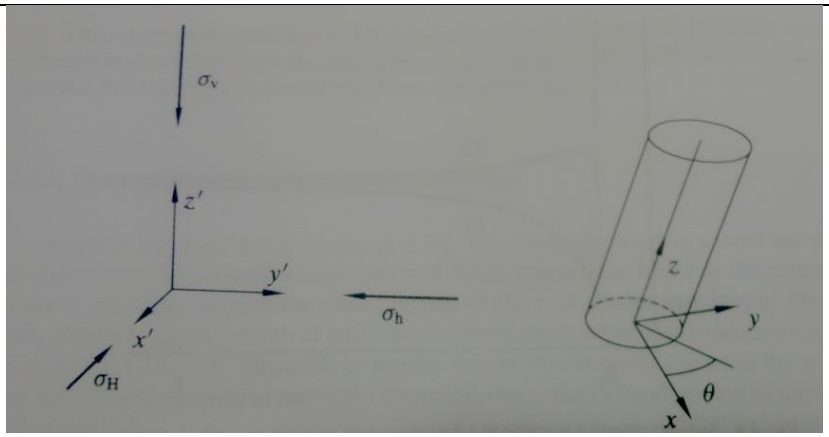

Figure ii: Coordinate system for deviated borehole (Fjær et al. 2008, 146)

Transformation formulas from page 146 (Fjær et al. 2008)

$$\begin{aligned} l_{xx'} &= \cos a \cos i, & l_{xy'} &= \sin a \cos i, & l_{xz'} &= -\sin i \\ l_{yx'} &= -\sin a, & l_{yy'} &= \cos a, & l_{yz'} &= 0 \\ l_{zx'} &= \cos a \sin i, & l_{zy'} &= \sin a \sin i, & l_{zx'} &= \cos i \end{aligned} \qquad \text{A1}$$

$$\sigma_x^0 = l_{xx'}^2\sigma_H + l_{xy'}^2\sigma_h + l_{xz'}^2\sigma_v \qquad \text{A2}$$

$$\sigma_y^0 = l_{yx'}^2\sigma_H + l_{yy'}^2\sigma_h + l_{yz'}^2\sigma_v \qquad \text{A3}$$

$$\sigma_z^0 = l_{zx'}^2\sigma_H + l_{zy'}^2\sigma_h + l_{zz'}^2\sigma_v \qquad \text{A4}$$

$$\tau_{xy}^0 = l_{xx'}l_{yx'}\sigma_H + l_{xy'}l_{yy'}\sigma_h + l_{xz'}l_{yz'}\sigma_v \qquad \text{A5}$$

$$\tau_{yz}^0 = l_{yx'}l_{zx'}\sigma_H + l_{yy'}l_{zy'}\sigma_h + l_{yz'}l_{zz'}\sigma_v \qquad \text{A6}$$

$$\tau_{zx}^0 = l_{zx'}l_{xx'}\sigma_H + l_{zy'}l_{xy'}\sigma_h + l_{zz'}l_{xz'}\sigma_v \qquad \text{A7}$$

Appendix B: Pore pressure gradients from wells around the Butch salt dome

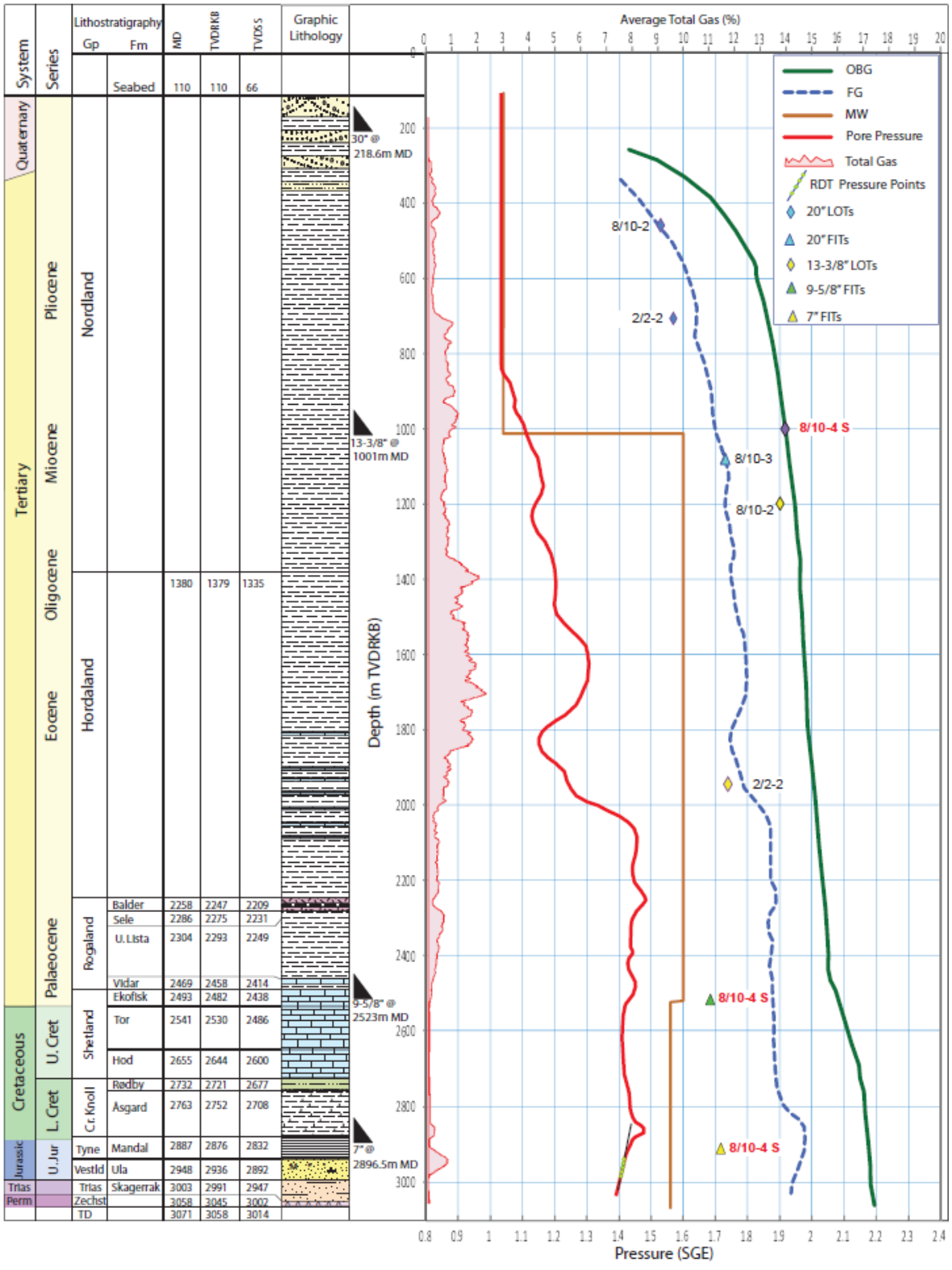

Figure iii: Pore pressure & fracture gradient interpretation for well 8/10-4S, Butch(centrica et al. 2012).

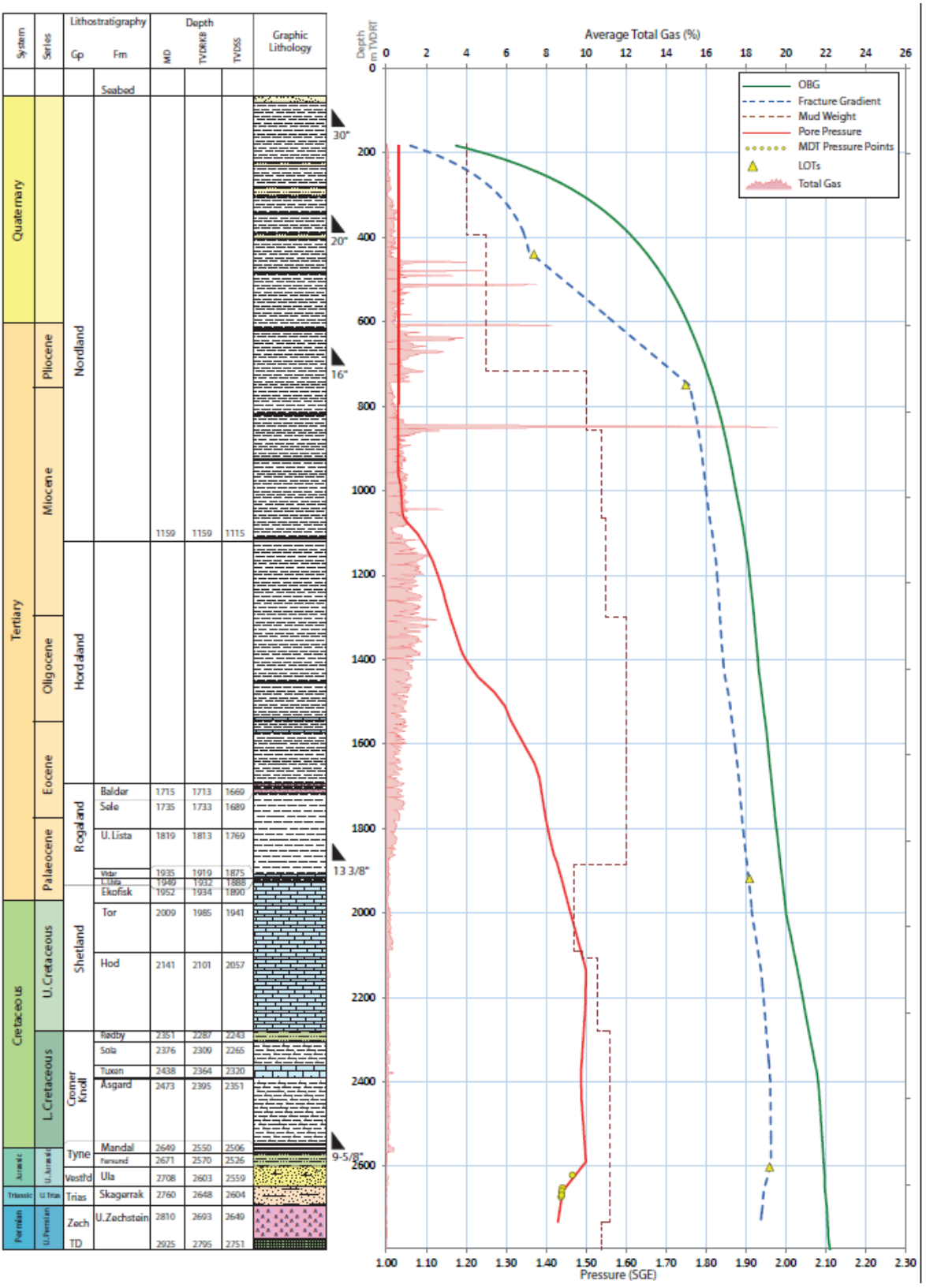

Figure iv: Pore pressure & fracture gradient interpretation for well 8/10-5S, Butch (centrica et al. 2014a).

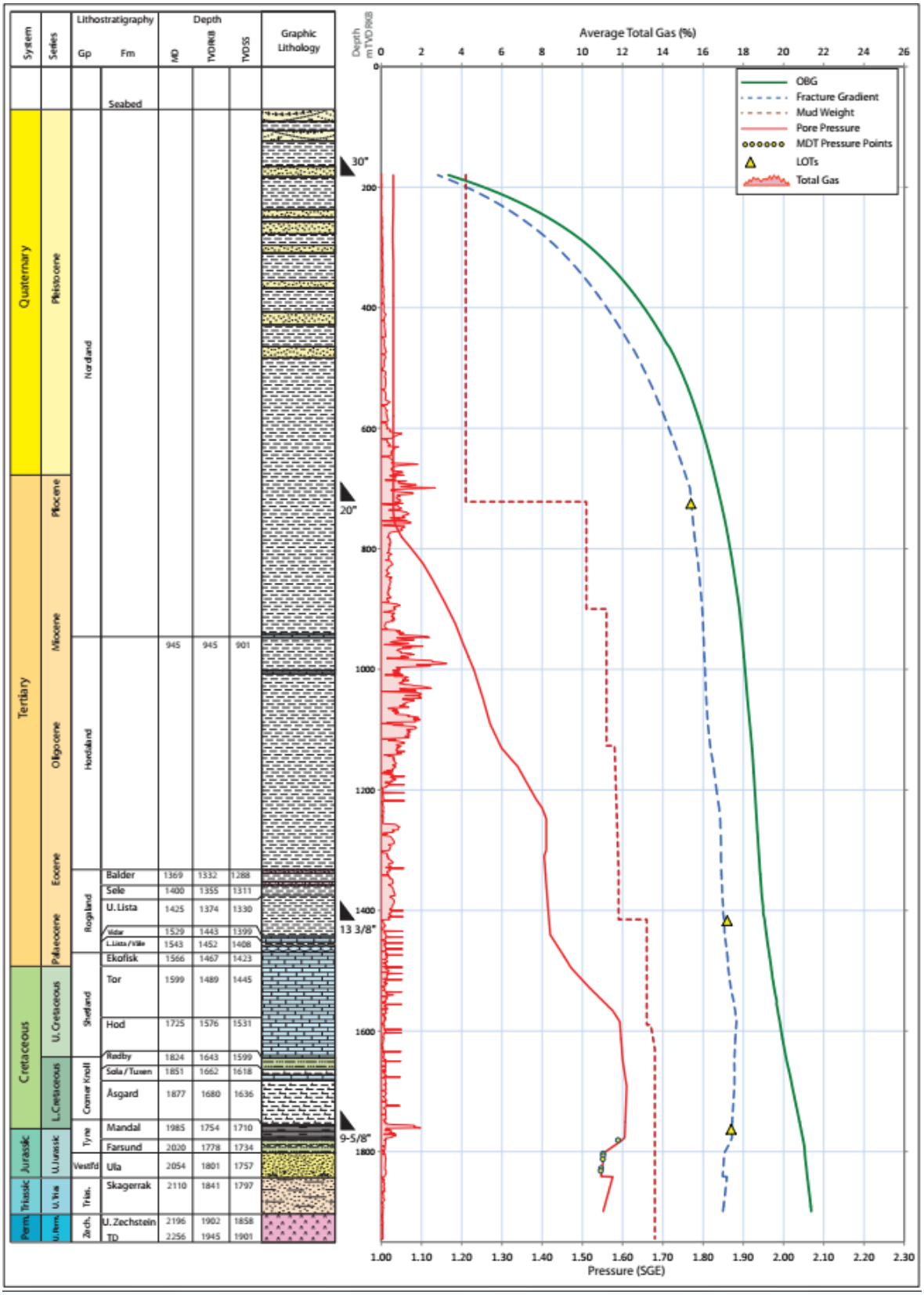

Figure v: Pore pressure & fracture gradient interpretation for well 8/10-6S, Butch (centrica et al. 2014b).